Relativistic band structure and spin-orbit splitting of zinc-blende-type semiconductors

M. Cardona, N. E. Christensen, and G. Fasol
Max-Planck-Institut für Festkörperforschung, Heisenbergstrasse 1, D-7000 Stuttgart 80, Federal Republic of Germany
(Received 16 November 1987)

Zinc-blende-type semiconductors differ from their diamondlike counterparts by the absence of inversion symmetry. This produces a number of spin splittings and spin-orbit coupling effects which are absent in the latter. For instance, all states at a general **k** are split by spin-orbit interaction. Also, bonding and antibonding *p*-like states are coupled by the same interaction. Many of these effects are calculated here on the basis of the *ab initio* self-consistent fully relativistic linear-muffin-tin-orbital method. For a better understanding and interpretation of the results, semiempirical parametrized 16×16 $\mathbf{k}\cdot\mathbf{p}$ calculations of several types are performed. Particular emphasis is placed on determining the signs of these splittings in an unambiguous manner. The results are compared with available experimental data of rather diverse origin.

I. INTRODUCTION

Spin-orbit interaction is known to split orbital degeneracies of band states, especially at high-symmetry points of the Brillouin zone (BZ) of cubic solids. In the tetrahedral semiconductors of germanium (diamond) and zinc-blende structure, such splittings appear in the top valence bands at Γ, L, and X, and for the *p*-like conduction bands at the same points.[1] They follow systematic trends related to the spin-orbit splitting of the valence *p* levels of the constituent atoms.[2] In fact, the experimental observation of such splittings, usually in the form of doublets in optical spectra, has been highly instrumental in the identification of electronic excitation spectra in terms of interband transitions.[2–4] The splittings at Γ and L appear both in Ge and zinc-blende-type materials, while the splitting at X occurs only for those of zinc-blende type, i.e., compounds with different anion and cation constituents. All states at Γ, L, and X, however, remain at least doubly degenerate. This degeneracy corresponds to the Kramers degeneracy.

The Kramers degeneracy requires a spin state at a general **k** point to have the same energy as the opposite-spin state at $-\mathbf{k}$. If the crystal has inversion symmetry (germanium structure), all states at *a given* **k** are therefore doubly degenerate. The situation is more subtle for the zinc-blende structure, which lacks a center of inversion. In this case, only along $\langle 100\rangle$ (Δ direction) do all the states remain doubly degenerate. The states along $\langle 111\rangle$ may or may not split, depending on the irreducible representation in the double-group symmetry of the states (states of $\Lambda_{4,5}$ symmetry split, while Λ_6 does not).[5,6] For other **k**'s inside the Brillouin zone all states become nondegenerate, the splitting being, of course, the result of spin-orbit interaction. It is expected to be largest along the $\langle 110\rangle$ directions since they are centrally located with respect to the $\langle 100\rangle$ and $\langle 111\rangle$ directions along which all or most of the splittings vanish. The splittings can be seen in band calculations which include spin-orbit interaction.[1,7] They amount to less than ~0.250 meV. These values are usually too small to be read with accuracy from published dispersion relations.[7] Thus information on calculated values of this splitting as a function of **k** is rarely available (for exceptions, see Refs. 8–11).

This lack of theoretical information is even more acute for the spin splitting around the band extrema which determine the transport properties. These splittings are very small, usually of third order in k (the distance in k space to the extrema), although sometimes a linear term appears. The coefficients of these cubic and linear terms manifest themselves experimentally in a number of ways. We mention, for instance, the spin-relaxation time which can be measured in optical-pumping experiments by means of the Hanle effect[12–14] and other forms of polarized luminescence.[15,16] These k^3 terms also affect the strength of the electric-field-induced spin resonance and, based on this fact, the coefficient of the k^3 terms (called γ or δ_0 in the literature) has been determined in InSb,[17] including its sign.[18]

The spin splitting of the bands of the GaAs along [110] has also been observed in the elegant spin-polarized photoemission experiments of Riechert *et al.*[19] Moreover, it should be mentioned that splittings linear in k are often induced by application of a uniaxial stress.[20] Such splittings can also be observed by means of the Hanle effect.[14]

In this paper we present calculations of the spin-orbit splittings just mentioned performed with the linear-muffin-tin-orbitals (LMTO) method.[21,22] These calculations are to be regarded as *ab initio*, except for adjustment of gaps related to the use of the local-density functional (the so-called gap problem).[23] In order to understand the mechanisms and interactions which are responsible for the calculated splittings, we have also performed a $\mathbf{k}\cdot\mathbf{p}$ calculation based on a parametrized 16×16 Hamiltonian. We have also analyzed the $\mathbf{k}\cdot\mathbf{p}$ results by means of perturbation expansions around $\mathbf{k}=0$. Particular emphasis has been placed on a consistent determination of the sign of the splittings with respect to the double-group symmetry of the corresponding eigenstates. In Sec. II we describe the $\mathbf{k}\cdot\mathbf{p}$ Hamiltonian and the phase choice for the eigenstates involved. We also discuss the sign of the matrix elements of **p** and introduce the off-diagonal spin-

orbit coupling Δ^- between p-like valence and conduction bands (Γ^v_{15} and Γ^c_{15}).[24] In Sec. III we present the band structures of InP, GaSb, InAs, ZnSe, and CuBr calculated with the LMTO method. In Sec. IV we compare the values of Δ^- obtained with three different methods: LMTO, LCAO (linear combination of atomic orbitals), and $\mathbf{k}\cdot\mathbf{p}$. In Sec. V we discuss the part of the spin splittings along [110] which is proportional to k^3 for small k. Results are presented for the Γ^v_{15} and Γ^c_{15} bands and the lowest conduction bands at Γ (Γ_1), as obtained with the LMTO and $\mathbf{k}\cdot\mathbf{p}$ methods. Emphasis is placed in giving the sign of these splittings in a unique, meaningful way. In Sec. VI we present the strain-induced linear splittings as obtained by $\mathbf{k}\cdot\mathbf{p}$ perturbation theory. In Sec. VII we discusses linear terms in k found in the Γ^v_{15} and Γ^c_{15} bands in the absence of strain. By means of LMTO calculations these terms are shown to be due to interactions with the core levels. Thus they do not appear in the $\mathbf{k}\cdot\mathbf{p}$ Hamiltonian. Their signs are also determined in an unambiguous fashion. The calculations are compared with the few experimental data available. These results are summarized in Sec. VIII. Finally, the Appendix contains some details of the $\mathbf{k}\cdot\mathbf{p}$ matrix.

II. THE $\mathbf{k}\cdot\mathbf{p}$ HAMILTONIAN

The $\mathbf{k}\cdot\mathbf{p}$ method is most commonly used to obtain the perturbation expansion, quadratic in k, of bands around high-symmetry points.[25–28] It can also be used to find the nonparabolic behavior for larger k by diagonalizing a truncated $\mathbf{k}\cdot\mathbf{p}$ Hamiltonian matrix.[6,8,25–30] We use here the 14×14 Hamiltonian of Ref. 25 enlarged to include one more s-like (Γ'_1) conduction band. The parameters of this 16×16 Hamiltonian appear in the eigenvalues of the 16 states at Γ (including their spin-orbit splittings), the matrix elements of $\mathbf{p}$, and the spin-orbit-coupling constant Δ^- between the Γ^v_{15} and the Γ^c_{15} bands.[8] The matrix elements of $\mathbf{p}$ are affected by the choice of the phases of the orbital wave functions and so is Δ^-. The latter, and some of the matrix elements of $\mathbf{p}$, reverse sign if the positions of the two atoms in the unit cell are interchanged. Hence, great attention must be paid to a consistent definition of all these parameters. We discuss it in detail below. The parameters used for our $\mathbf{k}\cdot\mathbf{p}$ calculations, performed for GaAs, GaSb, InP, and InSb, are listed in Table I. Many of the gaps and the spin-orbit splittings were obtained directly from experiments, while others were obtained by fitting experimental data or from some of our calculations (e.g., Δ^-, as will be presented below).

The following matrix elements of $\mathbf{p}$ appear in our Hamiltonian:

$$P=i\langle\Gamma^v_{15,x}\,|\,p_x\,|\,\Gamma_1\rangle\ ,\quad P'=i\langle\Gamma^c_{15,x}\,|\,p_x\,|\,\Gamma_1\rangle\ ,$$
$$P'''=i\langle\Gamma^v_{15,x}\,|\,p_x\,|\,\Gamma'_1\rangle\ ,\quad Q=i\langle\Gamma^v_{15,x}\,|\,p_y\,|\,\Gamma^c_{15,z}\rangle\ . \tag{2.1}$$

We use the definitions of Eq. (2.1) and the choice of wave-function phases (all real) and atomic origin given in Fig. 1 (from Ref. 31). Note that the *anion* has been chosen to be at the origin, while the *cation* is at $(a_0/4)(1,1,1)$. The opposite convention is often found in the literature, a fact which results in the sign reversal of P'.

Within the convention of Fig. 1 it is easy to see, simply by replacing p_x by $-i\partial/\partial_x$ and making rough sketches of the wave functions of Fig. 1 and their derivatives, that P, P', and Q are positive. We have not bothered to fix the phase of the second s-like conduction state Γ'_1 since this phase choice does not affect any other parameters of our Hamiltonian. The calculated bands are thus independent of the choice of sign of P'''. We use for P''' in GaAs the

TABLE I. Parameters used for the 16×16 $\mathbf{k}\cdot\mathbf{p}$ Hamiltonian (see the Appendix).

		GaAs	InP	GaSb	InSb
E_0 (eV)	Γ^c_6-Γ^v_8	1.519	1.424	0.813	0.235
Δ_0 (eV)	Γ^v_8-Γ^v_7	0.340	0.108	0.75	0.803
E'_0 (eV)	Γ^c_7-Γ^v_8	4.488	4.6	3.3	3.39
Δ'_0 (eV)	Γ^c_8-Γ^c_7	0.171	0.50	0.33	0.39
Δ^- (eV)	off-diagonal spin-orbit splitting	−0.085	0.22	−0.28	−0.244
E'''_0 (eV)	Γ'_6-Γ^v_8	9.18	9.66	7.27	6.78
P (a.u.)	$\langle\Gamma^v_{15,x}\,\vert\,p_x\,\vert\,\Gamma_1\rangle$	0.692	0.601	0.660	0.661
P' (a.u.)	$\langle\Gamma^c_{15,x}\,\vert\,p_x\,\vert\,\Gamma_1\rangle$	0.331	0.299	0.231	0.220
P''' (a.u.)	$\langle\Gamma^c_{15,x}\,\vert\,p_x\,\vert\,\Gamma'_1\rangle$	0.695	0.243	0.556	0.42
Q (a.u.)	$\langle\Gamma^c_{15,y}\,\vert\,p_x\,\vert\,\Gamma^v_{15z}\rangle$	0.47	0.503	0.564	0.571
C_k (a.u.)	k-linear term valence band	−0.000 25	−0.0001	0.000 03	−0.000 64
C'_k (a.u.)	k-linear term upper conduction band	0.000 21	−0.000 08	0.000 79	0.000 79
γ_1	Luttinger parameter	6.85	5.05	13.2	40.1
γ_2	Luttinger parameter	2.10	1.6	4.4	18.1
γ_3	Luttinger parameter	2.90	1.73	5.7	19.2
a_0 (Å)	lattice constant	5.65	5.869	6.082	6.479

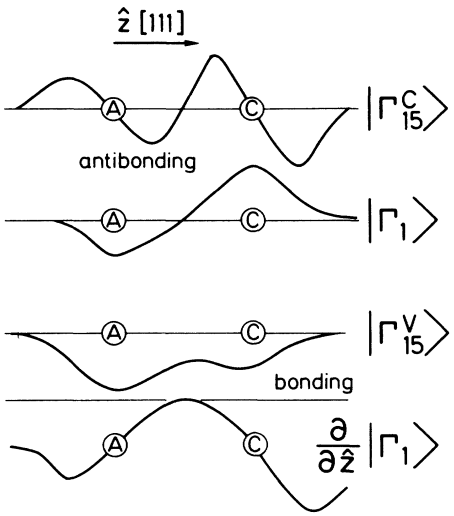

FIG. 1. Schematic diagram giving the phases of the Γ_{15}^{c}, Γ_1, and Γ_{15}^{v} wave functions used in this work. A and C represent cation and anion. For the p-like functions $\Gamma_{15}^{c,v}$ the component of $\hat{\mathbf{z}}$ symmetry ($\hat{\mathbf{z}}\|[111]$) is depicted.

value $P'''=0.66$ bohr^{-1} calculated with the pseudopotential Hamiltonian of Ref. 30. For the other materials we have slightly reduced P''' so as to obtain spin splittings of the Γ_{15}^{v} band along [110] close to the LMTO results (see below). The $\mathbf{k}\cdot\mathbf{p}$ matrix elements between Γ_{15}^{v} states have been written in terms of the Luttinger parameters γ_1, γ_2, and γ_3, related to the P, P', Q,[32] and interactions with other bands not contained in our basis (Löwdin perturbation theory). These matrix elements are given in the Appendix.

The spin-orbit-coupling parameter Δ^- is real if Γ_{15}^{v} and Γ_{15}^{c} are chosen as real, following the phase convention of Fig. 1. We define Δ^- as

$$\Delta^- = 3\langle (\tfrac{3}{2}\tfrac{3}{2})_v \,|\, H_{\text{s.o.}} \,|\, (\tfrac{3}{2}\tfrac{3}{2})_c \rangle \ , \tag{2.2}$$

where $(\frac{3}{2}\frac{3}{2})$ represents the angular-momentum-like eigenvector of the Γ_{15}^{v} eigenstates plus spin. The parameters C_k and C_k' represent the splittings of the Γ_{15}^{v} and Γ_{15}^{c} bands (Γ_8 component) linear in k (see Sec. VII).

The energies of the E_0''' gap ($\Gamma_8^v \rightarrow \Gamma_1'$) were taken from our LMTO calculations. We note that in the case of GaAs the calculated value (9.18 eV) is somewhat higher than the experimental one (8.24 eV).[33,34] The other energies of Γ states and the diagonal spin-orbit-splitting matrix elements were taken from experimental data[33] or, in the case of the latter, from LMTO calculations when the experimental data did not look convincing. The following procedure was used to fix the values of P, P', and Q. A relationship between P and P' was derived in the manner indicated in Ref. 26:

$$P'^2 = P^2 \frac{E_0' - E_{0c}'}{E_0' + E_{0c}'} \ , \tag{2.3}$$

where E_{0c}' represents the Γ_{15}-Γ_1 gap of the isoelectronic group-IV material. Typically, $P' \simeq 0.35P$. The value of P is then fixed so as to obtain, with the equation[26–28]

$$\frac{1}{m_c^*} = 1 + 2P^2 \left[\frac{1}{3} \left(\frac{2}{E_0} + \frac{1}{E_0 + \Delta_0} \right) + \left(\frac{P'}{P} \right)^2 \frac{1}{E_0' - E_0} \right] , \tag{2.4}$$

the experimental value m_c^* of the electron mass at Γ_6^c. [Equation (2.4) is in atomic units, $m = e = \hbar = 1$.] In this way we avoid the use of the artificial additive parameters C and C' introduced in Ref. 28. (Note, however, that recent magneto-Raman experiments[35] require a value of $C \simeq -1.7$ for GaAs. When more information becomes available for other materials, it can be simply incorporated into our $\mathbf{k}\cdot\mathbf{p}$ calculations.) The matrix element Q was obtained from the Luttinger parameters γ_1 and γ_2 with the expression (see the Appendix)

$$2Q^2 = (\gamma_1 - 2\gamma_2 + 1)(E_0' + \tfrac{2}{3}\Delta_0') \ . \tag{2.5}$$

Our parameters thus reproduce the experimental m_c^* by construction: The coupling through Δ^- affects m_c^* only negligibly. It affects, however, the corresponding effective g_c^* factor through a third-order perturbation term:[36,37]

$$\Delta g_c^* = \frac{8}{9} \frac{\Delta^- P P'}{E_0' - E_0} \left(\frac{1}{E_0} + \frac{2}{E_0 + \Delta_0} \right) . \tag{2.6}$$

This contribution amounts to -1.7 in InSb and plays an important role in the magnetic field dependence of the spin splitting.[36,37] We show in Table II the values of Δg_c^* and the total g_c^* calculated for GaAs, GaSb, InP, and InSb and compare them with experimental results. The corresponding effective masses m_c^* are also given for those materials plus ZnSe and CdTe. We present in Table III the effective masses of those six semiconductors.

TABLE II. Values of the electron g factor g_c^* obtained with the $\mathbf{k}\cdot\mathbf{p}$ method compared with experimental results. The corresponding m_c^*, which agrees with experiment by construction, is also given and compared with the results of the LMTO calculation. Δg_c^* represents the contribution of the Γ_{15}^{v}-Γ_{15}^{c} spin-orbit coupling to g_c^*. It has been found experimentally to be -1.7 for InSb, in excellent agreement with the calculated values (Ref. 36).

	$\Delta g_c^{*\,a}$	$g_c^{*\,a}$	$g_c^{*\,b}$	$m_c^{*\,a,b}$	$m_c^{*\,c}$
GaAs	−0.28	0.43	0.44	0.067	0.095[d]
GaSb	−0.8	−8.2	−9.1	0.041	0.050
InP	+0.6	−1.8	−1.5	0.078	0.101
InSb	−1.7	−52.7	−51.3	0.014	0.016
ZnSe			−1.7	0.14	0.160
CdTe			1.1	0.090	0.099

[a]Calculated, $\mathbf{k}\cdot\mathbf{p}$.
[b]Experimental, from Ref. 33.
[c]Calculated, LMTO.
[d]The value 0.068 given in Ref. 47 was obtained by using a slightly more optimized set of adjusting potentials.

TABLE III. Effective masses of the Γ_1 and Γ_{15}^v bands of GaAs, GaSb, InP, InSb, ZnSe, and CdTe as obtained with the LMTO and $\mathbf{k}\cdot\mathbf{p}$ methods ($\mathbf{k}\|[110]$), compared with experimental results, for $\mathbf{k}\|[110]$ and [111] from Ref. 33.

		GaAs	GaSb	InP	InSb	ZnSe	CdTe
$m_{\rm lh}^*$	$\mathbf{k}\cdot\mathbf{p}$	0.085	0.044	0.13	0.017		
	LMTO	0.096	0.06	0.10	0.019	0.15	0.08
	Expt.	0.082	0.042	0.12	0.016	0.14	0.11
$m_{\rm hh}^*$	$\mathbf{k}\cdot\mathbf{p}$	0.73	0.45	0.66	0.49		
	LMTO	0.61	0.41	0.52	0.49	0.88	0.87
	Expt.	0.57	0.37	0.60	0.45	1.1	0.83
$m_{\rm s.o.}^*$	$\mathbf{k}\cdot\mathbf{p}$	0.18	0.13	0.20	0.098		
	LMTO	0.20	0.10	0.18	0.15	0.28	0.26
	Expt.	0.17	0.13	0.12			

III. LMTO BAND-STRUCTURE CALCULATIONS

The electronic band structures of the compound semiconductors can efficiently be calculated by means of the LMTO method, although this method is particularly suited for close-packed crystal structures. However, by introducing at the interstitial positions in the sphalerite structure so-called "empty spheres," i.e., atomic spheres without nuclear charge, this open structure is converted into a close-packed one. Consequently, the errors in the LMTO are minimized. It has been demonstrated[21] that if an *ab initio* pseudopotential and a LMTO calculation use the same principles for construction of the potentials, then the same band structures of the zinc-blende-type semiconductors are obtained. At first, this may seem surprising since the pseudopotential method does not, as the LMTO does, apply spherically symmetrized potentials. It is, however, the introduction of the "empty spheres" in this "atomic-sphere approximation" (ASA) that provides an additional variational degree of freedom which is sufficient to compensate for the omission of the intra-atomic polarization effects. The close agreement between the LMTO and pseudopotential semiconductor band structures is only found, though, when the LMTO includes the so-called "combined correction term."[38] Further, these observations only apply to compounds in the perfect- (high-symmetry) crystal structures. If accurate LMTO calculations are to be performed for distorted structures—for example, with the purpose of obtaining deformation potentials relating to uniaxial strains, or optical-phonon frequencies—then the ASA form of the potential is too simplified. Methods that go beyond the ASA, and thus can treat these more complex problems, are presented elsewhere.[39–41]

An important advantage of the LMTO method over some of the other first-principles schemes is that it requires only a small set of basis functions. It applies a partial-wave representation. The version which we use here needs, in order to ensure a sufficient angular-momentum convergence, the inclusion of *s*, *p*, and *d* components. Although not strictly necessary on the empty spheres, we include these on all sites. The fact that we have to include the *d* partial waves in any case also implies that we, without any additional computational effort, can include the outer cation *d* states as fully relaxed band states. The *d* states affect the band structure also at the top of the valence band. Even in GaAs, where the Ga 3*d* states are relatively low, their influence is nonnegligible. In ZnSe, where the cation *d* states are considerably higher in energy, the influence on the valence-band structure becomes much more pronounced; they cause the VBM to shift upwards by ≈ 0.6 eV, as compared to a calculation where the Zn 3*d* states are treated as ("frozen," renormalized) corelike states. The band structure of CuBr, where the Cu 3*d* band intersects the Br bonding *p* bands, is even qualitatively erroneously described if these *d* states are not included.

Some of the band-structure features which we wish to describe in the present work, the *k*-linear splittings, are, in part, determined by the hybridization between the cation *d* states and the valence states. Thus, it is essential that these states are properly included in the LMTO scheme. The splittings are also influenced by the anion corelike states. These are, however, lying so low in energy that they can safely be treated as atomiclike. Their effect is still felt by the valence bands since, in the LMTO, the valence states satisfy the requirement of being orthogonal to all core states.[38]

The splittings of the bands in the zinc-blende-type crystals are caused by the spin-orbit (s.o.) interaction. Therefore, this is included in the LMTO scheme. It may be done either by adding a s.o. part formally as a perturbation to the "scalar"-relativistic Hamiltonian, or by using, as we prefer here, a fully Dirac-relativistic formulation.[42,43] In both cases, this implies that all matrices (Hamiltonian, overlap, etc.) are doubled in size. With *s*, *p*, and *d* partial waves included in the basis set on all sites, the matrix dimensions are 72×72 (four "atoms" in the basis). The crystal potentials are calculated by iterating the one-electron wave equation to self-consistency with an effective potential where exchange correlation is treated in the local-density approximation (LDA) plus additional potentials (see below). For the LDA we use the form constructed by Ceperley and Alder[44] as parametrized by Perdew and Zunger.[45] The relativistic

corrections suggested by McDonald and Vosko[46] are included.

It is well known that the band structures which formally are obtained from the one-particle energies of the wave equation in the LDA for semiconductors and insulators have gaps that are far too small (see, e.g., Ref. 38). In the present work, where we wish to calculate spin splittings, such errors are not acceptable since they produce incorrect values of the splittings in the conduction bands. The band structures that we use must therefore have conduction bands that are correctly located in energy with respect to the valence bands. It is not sufficient to shift them rigidly so as to adjust the minimum gap: this correction would preserve the wrong dispersion. A simple *ad hoc* procedure that simultaneously corrects the gaps and the dispersion was applied earlier,[47] and consists of adjusting the gaps at three symmetry points, Γ, X, and L, by introducing "false Darwin shifts." This is done by adding to the effective potentials an additional external potential, $V_\omega(\mathbf{r})$, that is sharply peaked at the atomic sites. We take this potential to be of the form

$$V_\omega(r)=V_0\left[\frac{r_0}{r}\right]\exp[-(r/r_0)^2]\ , \tag{3.1}$$

in the atomic sphere considered. These potentials are added on the real-atom sites as well as on those of the empty spheres. The parameters V_0 and r_0 are different on the various sites. The range parameters, r_0, are chosen so small that mainly the s-like states are affected. With these extra terms added to the LDA effective potential, the LMTO calculations are iterated to self-consistency. The valence states and the ground-state properties (theoretical equilibrium volume, etc.) are only slightly affected by the extra, δ-function-like potentials. It is interesting to note that, since they are included self-consistently, they do not only affect the lowest s-like conduction band, but also the higher states. The optical spectra derived from such "adjusted" band structures agree well[48] with experiments. There is, for a given semiconductor, no unique set of (V_0,r_0) parameters. Usually the r_0 values are chosen rather arbitrarily, and keeping them fixed the four V_0 parameters are varied until the gaps are sufficiently well reproduced, either by "trial and error" or by a simple self-consistency scheme. The parameters we have used for the compounds considered here are given in Table IV.

The band structures of GaAs, GaSb, InP, InSb, CdTe, ZnSe, and CuBr as calculated according to the description above are shown in Figs. 2–8. The spin-orbit splittings calculated for the Γ_{15}^v, L_3^v, and Γ_{15}^c states, respectively, are listed in Table V. (See also Fig. 2 for the definitions.) These values differ only slightly from the splittings obtained without the potentials of Eq. (3.1). The pure LDA calculations[49] give for GaAs, InP, and CdTe the following values of Δ_0: 0.363, 0.123, and 0.931 eV, respectively.

In order to illustrate the range of validity in $\mathbf{k}$ space of the $\mathbf{k}\cdot\mathbf{p}$ perturbation calculation, we have plotted in Fig. 9 the LMTO as well as the $\mathbf{k}\cdot\mathbf{p}$ bands of GaSb (the Ga $3d$ bands are not included in this figure).

Since the sphalerite structure does not have inversion symmetry, several bands split due to the spin-orbit coupling as mentioned in the Introduction. Only few bands along particular symmetry lines ([111] and [100]) can maintain the twofold degeneracy. Some of the splittings are small, though, and therefore not easy to discern in the band-structure plots, Figs. 2–8. Therefore we show, on enlarged scales, a few examples of bands where the splittings can be seen more clearly. First, Fig. 10 shows for ZnSe the valence-band maximum and a part of the heavy-hole (hh), light-hole (lh), and split-off hole (sh) bands (for notation, see Fig. 6) along the Σ ([110]) line. In Fig. 11 the lowest conduction band, as well as the Γ_{15}^c-derived heavy-electron (he), light-electron (le), and split-off electron (se) bands are shown along the same symmetry line. As required by symmetry, the splittings vanish at Γ and X. The band structure becomes very complex in the $\mathbf{k}$ regime where the (he), (le), and (se) bands tend to cross, and therefore a consistent assignment of the splittings to specific bands, e.g., he, along the entire line from Γ to X is not possible. The quantities we shall derive and use here, however, will be obtained only from the k regions near Γ, and there the bands can be unambiguously identified. Such complications do not occur for the lowest conduction band, e, in ZnSe. Considering now the same bands, Figs. 12 and 13, along the Λ line ([111]), it is seen that only the hh and he bands split (the splitting of he can hardly be seen in Fig. 13). The lh, sh, le, and se states are doubly degenerate along this line. This is also the case for the lowest conduction band (not shown in these figures).

The splittings of the hh, lh, he, and le as well as the split-off bands of CuBr are illustrated in Figs. 14(a), 14(b), and 15 for $\mathbf{k}$ at the Σ line, and in Figs. 16 and 17 these bands are shown for $\mathbf{k}$ along the [111] direction. It fol-

TABLE IV. Parameters of the external potentials, V_0 (in hartrees) and r_0 (in bohrs), used with Eq. (3.1). E_1 and E_2 label the "empty" spheres, E_1 being the one surrounded by cations.

	Cation		Anion		E_1		E_2	
	V_0	r_0	V_0	r_0	V_0	r_0	V_0	r_0
GaAs	280.0	0.015	190.0	0.015	5.0	0.55	6.0	0.55
GaSb	295.0	0.015	245.0	0.015	5.0	0.45	5.7	0.55
InP	200.0	0.015	180.0	0.015	6.6	0.55	5.7	0.55
InSb	145.0	0.015	145.0	0.015	50.0	0.48	90.0	0.58
CdTe	275.0	0.015	275.0	0.015	5.4	0.45	5.4	0.45
ZnSe	355.0	0.015	355.0	0.015	7.3	0.45	7.8	0.45
CuBr	750.0	0.015	750.0	0.015	7.3	0.45	7.3	0.45

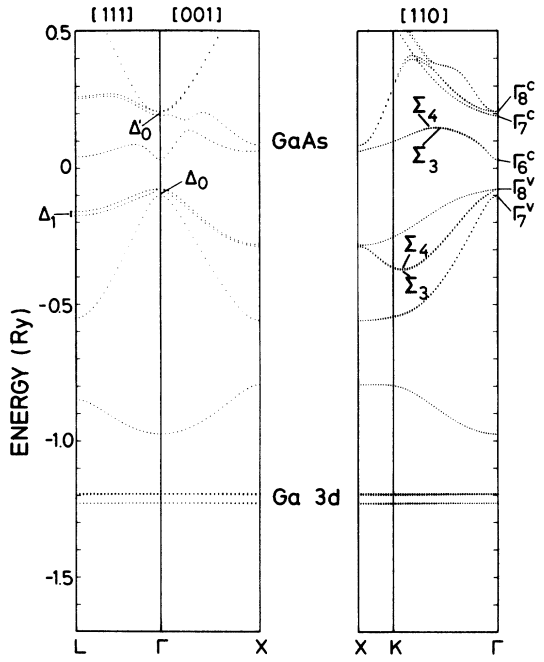

FIG. 2. Band structure of GaAs along symmetry lines as calculated in the local-density approximation (LDA), but with the adjusting potentials included self-consistently. Energies are given in rydbergs on the natural ASA energy scale; see, for example, Ref. 49. For details of spin splittings, see Fig. 22.

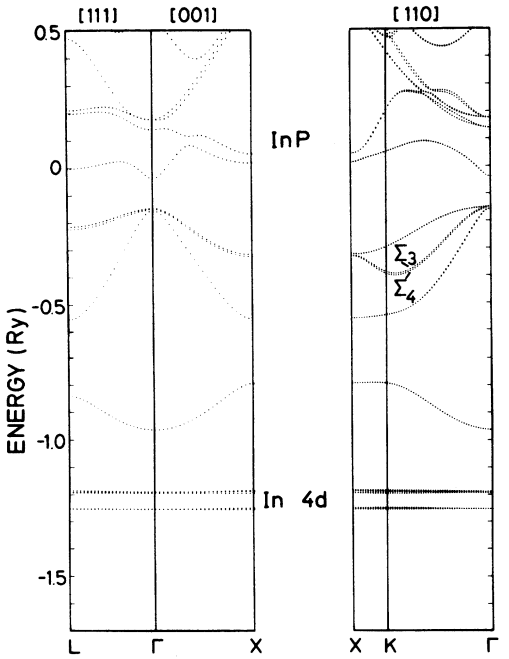

FIG. 4. Band structure of InP along symmetry lines as calculated in the LDA, but with the adjusting potentials included self-consistently. For details of spin splittings, see Figs. 24 and 29.

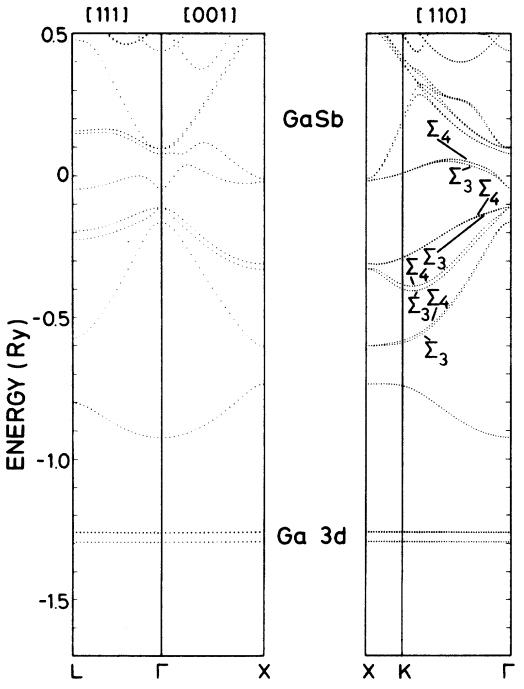

FIG. 3. Band structure of GaSb along symmetry lines as calculated in the LDA, but with the adjusting potentials included self-consistently. For details of spin splittings, see Figs. 23 and 28.

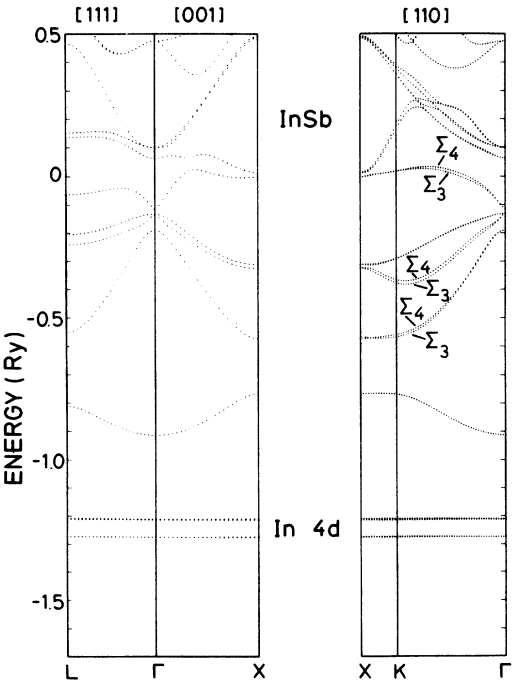

FIG. 5. Band structure of InSb along symmetry lines as calculated in the LDA, but with the adjusting potentials included self-consistently. For more details on spin splittings, see Fig. 25.

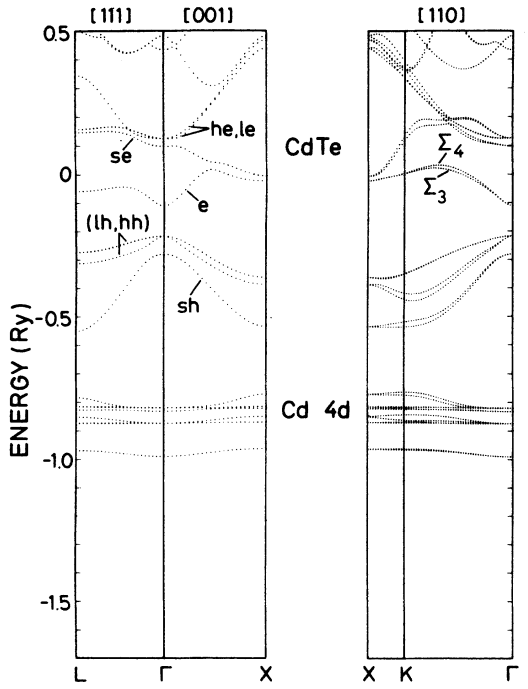

FIG. 6. Band structure of CdTe along symmetry lines as calculated in the LDA, but with the adjusting potentials included self-consistently. The labels, sh (split-off–hole), lh (light-hole), hh (heavy-hole), e (Γ_6-conduction-electron), le (light-electron), and he (heavy-electron) band, refer to the notation used in Sec. V. For details of spin splittings, see Fig. 27.

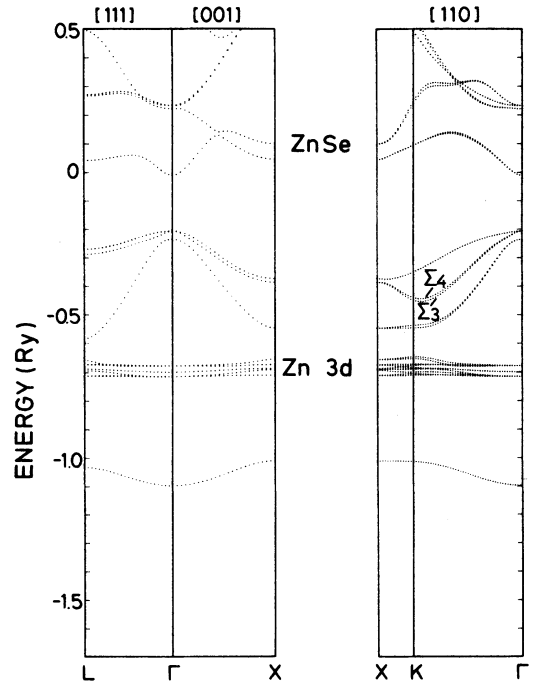

FIG. 7. Band structure of ZnSe along symmetry lines as calculated in the LDA, but with the adjusting potentials included self-consistently. For details, see Fig. 10.

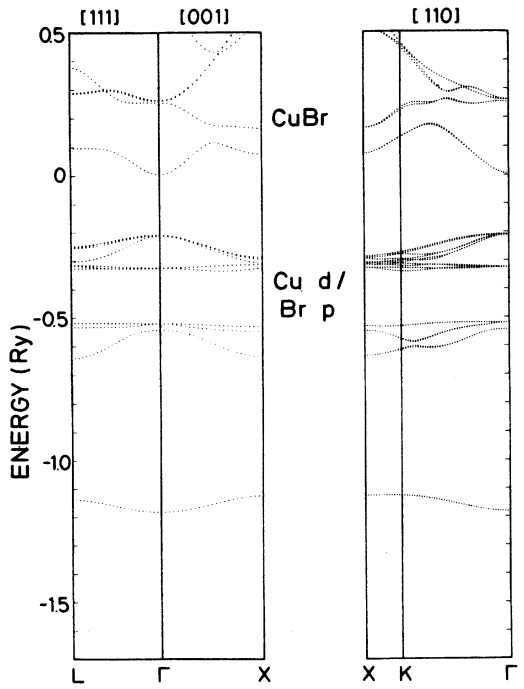

FIG. 8. Band structure of CuBr along symmetry lines as calculated in the LDA, but with the adjusting potentials included self-consistently. For details, see Figs. 15–17.

lows from Fig. 16 that the hh and lh bands cross even near Γ, and that a calculation of the k-linear terms therefore must be made with some care. The cases shown here are not the only ones where such difficulties were encountered [note also similar difficulties for the valence bands, Figs. 14(a) and 14(b)], and therefore it is often necessary to use a very dense k mesh to ensure that the coefficients of splittings are properly determined. We use up to 900 intervals on the Γ-L and Γ-K segments.

IV. ESTIMATES OF Δ^-

A. k·p estimates

The spin-orbit Hamiltonian couples the Γ_{15}^v and Γ_{15}^c states of a zinc-blende-type semiconductor since they are mainly p-like and have the same symmetry.[24] This cou-

TABLE V. Spin-orbit splittings at the valence-band maximum at Γ, Δ_0, at L, Δ_1, and of the conduction state Γ_{15}^c, Δ_0', as calculated by the LMTO method.

	Δ_0	Δ_1	Δ_0'
GaAs	0.351	0.213	0.178
GaSb	0.727	0.415	0.256
InP	0.120	0.126	0.499
InSb	0.799	0.497	0.497
CdTe	0.871	0.530	0.375
ZnSe	0.401	0.237	0.158
CuBr	0.044	0.073	0.111

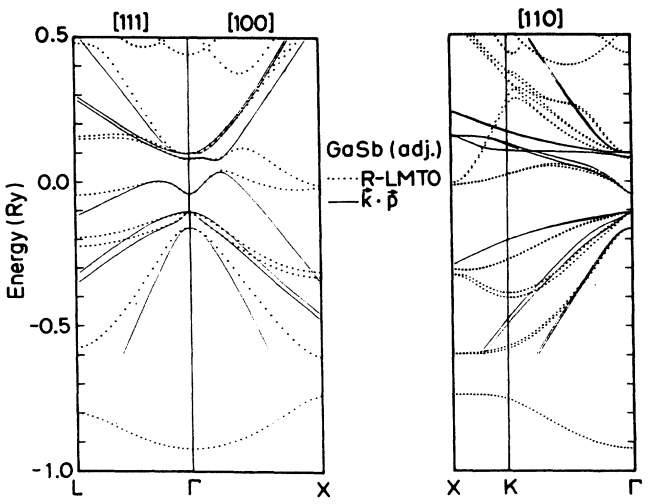

FIG. 9. LMTO (dots) and $\mathbf{k}\cdot\mathbf{p}$ (lines) band structures of GaSb. (Ga $3d$ bands not shown.) For details of spin splittings, see Fig. 23.

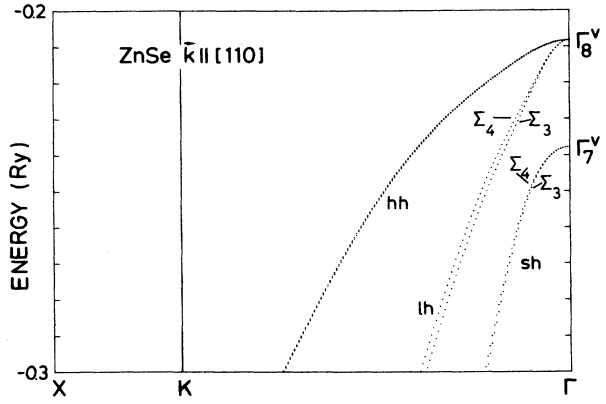

FIG. 10. ZnSe, relativistic LMTO band structure near the valence-band maximum for $\mathbf{k}$ along [110]. For more details, see Fig. 26.

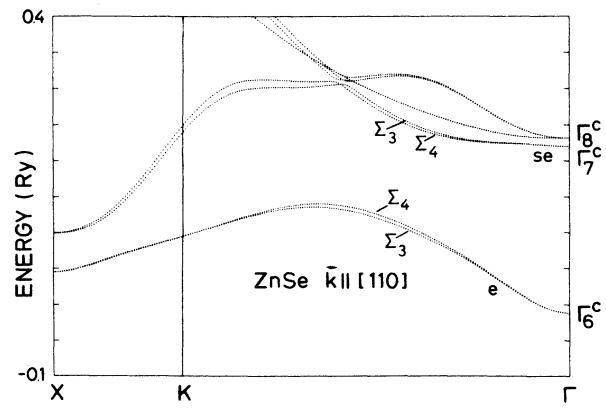

FIG. 11. ZnSe, like Fig. 10, but conduction bands along [110].

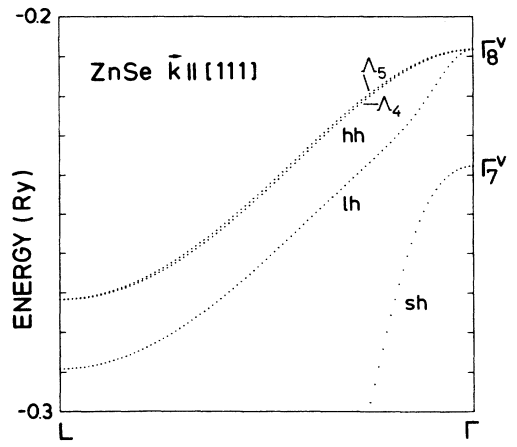

FIG. 12. ZnSe, relativistic LMTO band structure near the valence-band maximum for $\mathbf{k}$ along [111].

pling vanishes for diamond-type crystals: the state which corresponds to Γ_{15}^v ($\Gamma_{25'}$) is even (bonding), and that corresponding to Γ_{15}^c is odd (Γ_{15}, antibonding). Several methods can be used to estimate this coupling. Early estimates were published in Ref. 24 for GaAs, GaP, InP, and AlSb. Results for GaSb, InAs, InSb, ZnSe, and ZnTe can be found in Ref. 50. They were obtained through fits of various experimental spin-orbit splittings with a 30×30 $\mathbf{k}\cdot\mathbf{p}$ Hamiltonian. They are thus related to experimental data in a nontransparent manner. We reproduce the values for GaAs, GaSb, InP, and InSb in Table VI, where the sign of the coupling has been taken to conform with the choice of phases and atomic origin described above.

B. Tight-binding estimates

Another possible way of estimating Δ^- is based on a minimum-basis tight-binding method.[51] We assume that the Γ_{15}^v and Γ_{15}^c wave functions are obtained as bonding and antibonding linear combinations of p-like orbitals of the cation ($|\mathrm{III}\rangle$) and the anion ($|\mathrm{V}\rangle$):

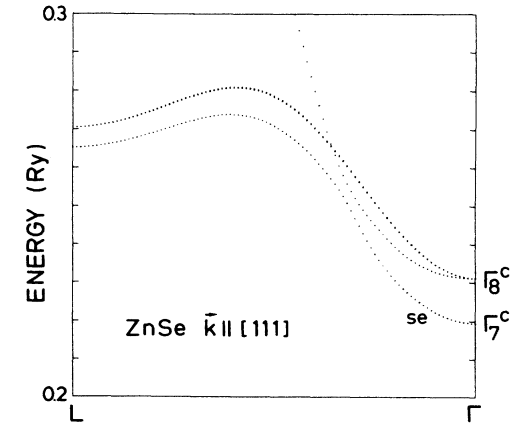

FIG. 13. ZnSe, like Fig. 12, but Γ_{15}^c-connected bands along [111].

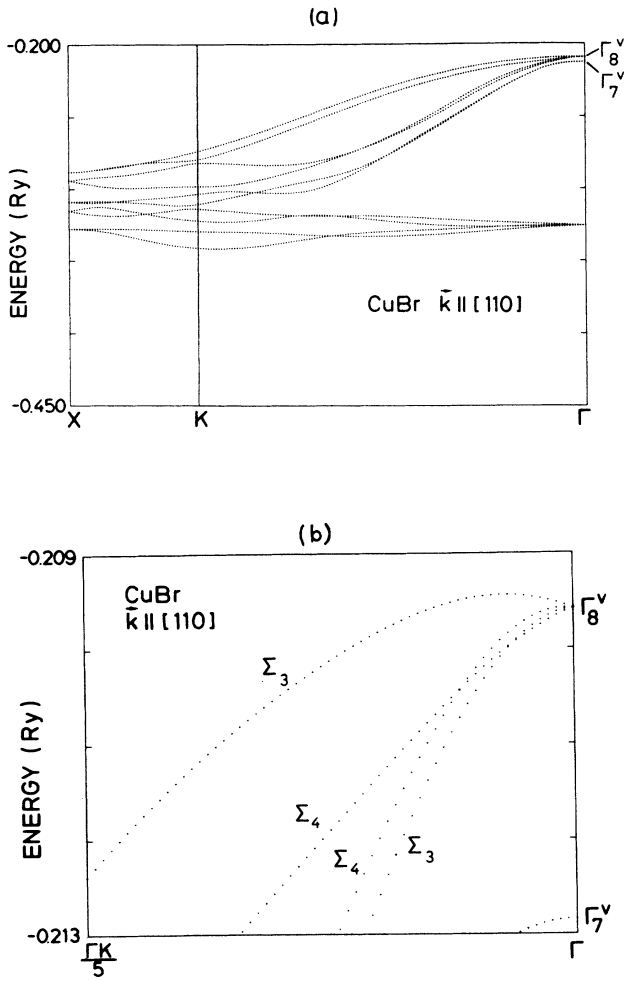

FIG. 14. CuBr, relativistic LMTO band structure near the valence-band maximum for **k** along [110]. Panel (b) shows a blow-up near the valence-band maximum.

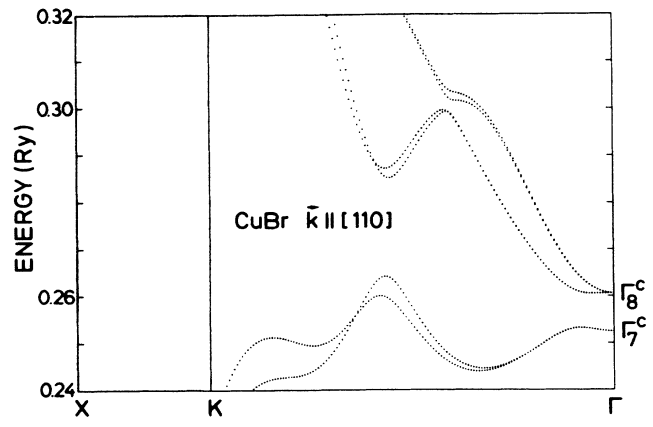

FIG. 15. CuBr, like Fig. 14, but Γ_{15}^{c}-connected bands along [110].

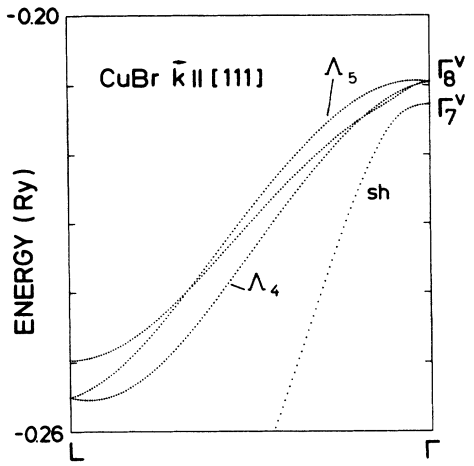

FIG. 16. CuBr, relativistic LMTO band structure near the valence-band maximum for **k** along [111].

$$|\Gamma_{15}^{v}\rangle=\alpha|\mathrm{V}\rangle+\beta|\mathrm{III}\rangle\ ,$$
$$|\Gamma_{15}^{c}\rangle=\beta|\mathrm{V}\rangle-\alpha|\mathrm{III}\rangle\ , \tag{4.1}$$

where we use for the $|\Gamma_{15}^{v,c}\rangle$ wave functions the phases of Fig. 1 and $|\mathrm{V}\rangle$ and $|\mathrm{III}\rangle$ both chosen to have the positive lobe to the right. Under these conditions $\alpha>0$ and $\beta<0$. Taking on- and off-diagonal matrix elements of the spin-orbit Hamiltonian, we find

$$\Delta^{-}=\alpha\beta(\Delta_{\mathrm{V}}-\Delta_{\mathrm{III}})\ , \tag{4.2a}$$
$$\Delta_0=\alpha^2\Delta_{\mathrm{V}}+\beta^2\Delta_{\mathrm{III}}\ , \tag{4.2b}$$
$$\Delta_0'=\beta^2\Delta_{\mathrm{V}}+\alpha^2\Delta_{\mathrm{III}}\ , \tag{4.2c}$$

where Δ_{V} and Δ_{III} are the atomic spin-orbit splittings, properly renormalized to take into account the compression of the atomic wave function in the core. Equations (4.2b) and (4.2c) are known to give reasonable values for Δ_0 and Δ_0'.[51] Equation (4.2a) can also be used to estimate Δ^{-} from the atomic splittings Δ_{V} and Δ_{III} and the admix-

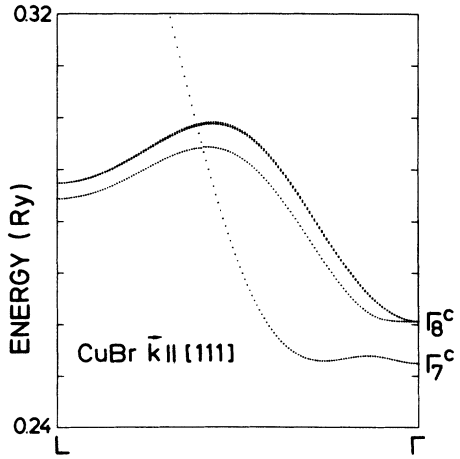

FIG. 17. CuBr, like Fig. 16, but Γ_{15}^{c}-connected bands along [111].

TABLE VI. Values of the spin-orbit parameter Δ^- which couples the Γ_{15}^c and Γ_{15}^v bands as obtained by the LCAO, **k·p**, and LMTO methods (see text). The sign of Δ^- is found with the two former methods but not with the latter method. We have assumed that the sign in this case is that obtained consistently with the **k·p** and LCAO methods.

	GaAs	GaSb	InP	InSb
k·p	−0.07	−0.4	+0.4	−0.014
LCAO	−0.085	−0.28	+0.16	−0.20
LMTO	−0.11	−0.32	+0.226	−0.244

ture parameters α and β obtained with standard prescriptions.[31,52] It is also possible to express Δ^- as a function of Δ_0 and Δ_0':

$$\Delta^- = \frac{\eta}{\eta^2-1}(\Delta_0-\Delta_0') , \tag{4.3}$$

where[31,52]

$$\eta=\frac{\alpha}{\beta}=\frac{-2H_{xx}}{E_{p\mathrm{III}}-E_{p\mathrm{V}}+[(E_{p\mathrm{V}}-E_{p\mathrm{III}})^2+4H_{xx}^2]^{1/2}} , \tag{4.4}$$

In Eq. (4.4), $E_{p\mathrm{III}}$ and $E_{p\mathrm{V}}$, both negative, are the diagonal elements of the tight-binding Hamiltonian (atomic-term values) and H_{xx} the overlap integral of bond length d with the expression[31,52]

$$H_{xx}=1.28d^{-2} . \tag{4.5}$$

For the materials under consideration here we find η to be around −2.4 (GaAs, −2.42; GaSb, −2.13; InP, −2.77; InSb, −2.46). Using experimental values of Δ_0 and Δ_0' given in Table I, we obtain the values of Δ^- shown in Table VI.

In spite of the agreement, in sign and magnitude, of these estimates of Δ^- with the other estimates of Table VI, a word of caution is due. While Eq. (4.2a) gives $\Delta^-=0$ for the diamond structure (replace $\Delta_{\mathrm{V}}=\Delta_{\mathrm{III}}$ since both atoms are equal), Eq. (4.3) does not. In Ge, for instance, $\Delta_0=0.29$ and $\Delta_0'=0.21$. This difference is mainly due to the fact that the Γ_{15}^c state has a considerable admixture of d-like orbitals (more so than Γ_{15}^v) which contribute little to the spin-orbit splitting. These orbitals have not been included in our tight-binding basis and thus will lead to errors in the estimate of Δ^-. We have tried to include them, however, and found no large changes in the estimate of Δ^-. We thus prefer to use Eq. (4.3) as it is, because of its simplicity and because of the agreement of the results obtained with those found by other methods (Table VI). Equation (4.3) shows that, for our choice of basis, $\Delta^-<0$ if $\Delta_0>\Delta_0'$ (GaAs, GaSb, InSb) and $\Delta^->0$ otherwise (InP).

C. LMTO estimates

In order to estimate Δ^-, we have calculated the Γ_{15}^v and Γ_{15}^c states both with the scalar-relativistic LMTO (i.e., s.o. coupling omitted) method and with its fully relativistic version. In the absence of Δ^- coupling, the Γ_{15} bands should split into $J=\frac{3}{2}$ and $\frac{1}{2}$ (Γ_8 and Γ_7) components, the shifts with respect to the scalar-relativistic value being in the ratio 2:1. The Δ^- coupling changes this ratio. In second-order perturbation theory we have for these shifts in the case of Γ_{15}^v (see Fig. 18)

$$\begin{aligned}\delta(\tfrac{3}{2})&=\frac{\Delta_0}{3}-\left[\left(\frac{\Delta^-}{3}\right)^2\Big/E_0'\right] ,\\ \delta(\tfrac{1}{2})&=-\frac{2\Delta_0}{3}-\left[\left(\frac{2\Delta^-}{3}\right)^2\Big/E_0'\right] .\end{aligned} \tag{4.6}$$

Thus, from the computed values of $\delta(\frac{3}{2})$ and $\delta(\frac{1}{2})$, we can determine both Δ_0 and Δ^- with Eq. (4.6). Δ_0 is only slightly changed from the value $\delta^{3/2}-\delta^{1/2}$ which would obtain for $\Delta^-=0$. In Table V we have actually listed for Δ_0 the directly computed values $\delta(\frac{3}{2})-\delta(\frac{1}{2})$. We list the values of Δ^- obtained in this manner in Table VI. The agreement in magnitude with the values obtained with the **k·p** and tight-binding methods is rather satisfactory. The LMTO procedure does not fix the sign of Δ^-. We have taken it to be that found with the other two methods.

In principle, Δ^- could also be determined from a relationship similar to Eq. (4.6) for the Γ_{15}^c band (Δ_0 replaced by Δ_0', E_0' by $-E_0'$). Such procedure yields values of Δ^- smaller than those found from Γ_{15}^v. We believe that the reason is the coupling of Γ_{15}^c to higher conduction bands, which tends to decrease the effect of Δ^-. In particular, the Γ_8^c component of Γ_{15}^c couples via $H_{\mathrm{s.o.}}$ to the Γ_{12}-orbital band (Γ_8^c in double-group notation, d-like) which is ~5.5 eV above Γ_{15}^c. Both Γ_8^c and Γ_7^c components of Γ_{15}^c couple to the next-higher Γ_{15} conduction bands, which are about 8 eV above Γ_{15}^c. In view of this, we have discarded the results obtained for Δ^- from Γ_{15}^c. The values of Δ^- in Table I represent a compromise among those of Table VI which give a reasonable results for the effects of Δ^- to be discussed below.

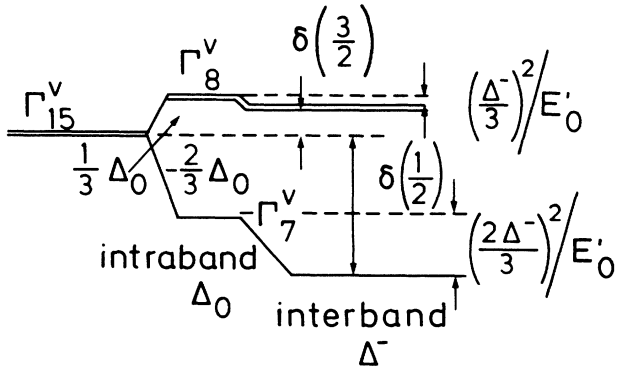

FIG. 18. Schematic diagram of the spin-orbit splitting of the Γ_{15}^v bands. The intraband terms (first-order perturbation theory) and their interband counterpart (second order) due to interaction with Γ_{15}^c are illustrated.

V. SPIN SPLITTING OF BANDS ALONG ⟨110⟩

A. Symmetries of the split bands

While in the diamond structure, as a result of the inversion symmetry, all states at a given $\mathbf{k}$ are doubly degenerate, this degeneracy is split in the zinc-blende structure at a general $\mathbf{k}$ point. Only along ⟨100⟩ do all states remain doubly degenerate.[5,6] Along ⟨111⟩ the double group has three representations: Λ_6, which is doubly degenerate, and Λ_4, Λ_5, which are complex conjugates of each other and may split. This splitting will be discussed in Sec. VII. Along ⟨110⟩ all states split. They belong to either of the two nondegenerate representations Σ_3 and Σ_4 (point group C_s). The double-group–character table of C_s is[53]

	E	$\bar{E}$	R	$\bar{R}$
Σ_3	1	-1	i	$-$i
Σ_4	1	-1	$-$i	i

(5.1)

where R represents, for $\mathbf{k}$ along [110], a reflection about the $(1\bar{1}0)$ plane. It is our purpose to give enough information to identify which of the two bands, that belonging to Σ_3 or that belonging to Σ_4, splits up in energy due to the spin-orbit interaction so as to attribute an unambiguous meaning to the sign of the splitting. Let us first consider the Γ_1 spin-up and -down states. They split for $\mathbf{k}\|[110]$. It is easy to check that the split eigenstates correspond to spin up and down with respect to the $[1\bar{1}0]$ direction. Let us determine which of these two states corresponds to Σ_3 and which to Σ_4 as defined in Eq. (5.1). We take $[110]\|\hat{\mathbf{z}}'$ as the quantization axis, together with $[001]\|\hat{\mathbf{x}}'$ and $[1\bar{1}0]\|\hat{\mathbf{y}}'$. The reflection, R multiplies the spin-up state along $[1\bar{1}0]$ ($\uparrow\hat{\mathbf{y}}'$) by $-i$ and the spin-down state ($\downarrow\hat{\mathbf{y}}'$) by i. Hence, $\uparrow\hat{\mathbf{y}}'$ belongs to Σ_4 and $\downarrow\hat{\mathbf{y}}'$ to Σ_3 according to Eq. (5.1). In the literature one usually finds the energy splitting given as positive when $\uparrow\hat{\mathbf{y}}'$ is above $\downarrow\hat{\mathbf{y}}'$. We keep this convention and extend it to the Γ_{15} states in the following way: the splitting will be thus designated as positive if the Σ_4 state is above the Σ_3 partner. We must now investigate the symmetry of the Γ_{15} states.

The simplest Γ_{15} set of states to consider is that with $J=\frac{1}{2}$ (Γ_7). These states have the form, referred to the $\hat{\mathbf{y}}'$ axis as axis of quantization,

$$
\begin{aligned}
&(\tfrac{1}{2},\tfrac{1}{2})_{\hat{\mathbf{y}}'}=\frac{1}{\sqrt{3}}[(\mathbf{Z}'+i\mathbf{X}')\downarrow+\mathbf{Y}'\uparrow]\,, && \text{belongs to } \Sigma_3\\
&(\tfrac{1}{2},-\tfrac{1}{2})_{\hat{\mathbf{y}}'}=\frac{1}{\sqrt{3}}[(\mathbf{Z}'-i\mathbf{X}')\uparrow-\mathbf{Y}'\downarrow]\,, && \text{belongs to } \Sigma_4\,.
\end{aligned}
\tag{5.2}
$$

By applying the R reflection to the wave functions of Eq. (5.2), it is easy to see that they belong to the representations given above. Hence their splitting will be given as positive when $(\frac{1}{2},-\frac{1}{2})$ have a higher energy than $(\frac{1}{2},\frac{1}{2})$.

We discuss next the sign convention for the Γ_8 ($J=\frac{3}{2}$) bands. For $\mathbf{k}$ along [001] and also [111] they split via quadratic terms in k (effective mass) into their $J_z=\pm\frac{3}{2}$ and $\pm\frac{1}{2}$ components. Their spin-split eigenstates can be easily recognized by the fact that they are invariant upon the reflection R. They are, for $(\frac{3}{2},\pm\frac{3}{2})$,

$$
\begin{aligned}
&\tfrac{1}{2}[(\mathbf{X}'+i\mathbf{Y}')\uparrow+i(\mathbf{X}'-i\mathbf{Y}')\downarrow]\,, && \text{symmetry } \Sigma_4\\
&\tfrac{1}{2}[(\mathbf{X}'+i\mathbf{Y}')\uparrow-i(\mathbf{X}'-i\mathbf{Y}')\downarrow]\,, && \text{symmetry } \Sigma_3
\end{aligned}
\tag{5.3}
$$

where the axis of quantization $\hat{\mathbf{z}}'$ is taken along $\mathbf{k}$. The Σ_4-Σ_3 symmetry identification given in Eq. (5.3) is that with respect to the (110) plane, the symmetry element common to the [001], [111], and also [110] directions. Since the states of Eq. (5.3) are degenerate for $\mathbf{k}$ along [111] and [001], the Σ notation provides a convenient way of labeling them. The corresponding functions derived from the $(\frac{3}{2},\pm\frac{1}{2})$ components of Γ_8^v are

$$
\begin{aligned}
&\frac{1}{\sqrt{2}}[(\tfrac{3}{2},\tfrac{1}{2})+i(\tfrac{3}{2},-\tfrac{1}{2})]\,, && \text{symmetry } \Sigma_3\\
&\frac{1}{\sqrt{2}}[(\tfrac{3}{2},\tfrac{1}{2})-i(\tfrac{3}{2},-\tfrac{1}{2})]\,, && \text{symmetry } \Sigma_4
\end{aligned}
$$

where (5.4)

$$
\begin{aligned}
(\tfrac{3}{2},\tfrac{1}{2})&=\frac{1}{\sqrt{6}}[(\mathbf{X}'+i\mathbf{Y}')\downarrow-2\mathbf{Z}'\uparrow]\,,\\
(\tfrac{3}{2},\tfrac{1}{2})&=\frac{1}{\sqrt{6}}[(\mathbf{X}'-i\mathbf{Y}')\uparrow+2\mathbf{Z}'\downarrow]\,.
\end{aligned}
$$

For $\mathbf{k}\|[110]$ the symmetry is lower and the $J_z=\pm\frac{3}{2}$ and $\pm\frac{1}{2}$ components mix with increasing $\mathbf{k}$: the eigenstates are no longer determined by symmetry, but by the solution of the $\mathbf{k}\cdot\mathbf{p}$ secular equation. In the case of Γ_8^v, however, the $\mathbf{k}\cdot\mathbf{p}$ interaction with Γ_1 via the matrix element P dominates. This interaction is isotropic, i.e., independent of the direction of $\mathbf{k}$. Hence, to a good approximation, the [110] wave functions are still $(\frac{3}{2},\pm\frac{3}{2})$ and $(\frac{3}{2},\pm\frac{1}{2})$ with [110] ($\hat{\mathbf{z}}'$) the direction of quantization. This is equivalent to saying that the set of the bands $(\frac{3}{2},\pm\frac{3}{2})$ is still heavy-hole-like, while the other is light-hole-like. This simple separation does not hold for the Γ_8^c bands: in this case the isotropic $\mathbf{k}\cdot\mathbf{p}$ interactions with matrix elements P' and P''', have opposite signs and the resulting bands are strongly anisotropic. The nearly isotropic case corresponds actually to $(\gamma_2-\gamma_3)/\gamma_1\ll 1$, where γ_1, γ_2, and γ_3 are the Luttinger parameters.

Let us consider the $(\frac{3}{2},\pm\frac{3}{2})$ bands in the nearly isotropic case. They can be written as

$$
\begin{aligned}
(\tfrac{3}{2},\tfrac{3}{2})&=\frac{1}{\sqrt{2}}(\mathbf{X}'+i\mathbf{Y}')\uparrow\,,\\
(\tfrac{3}{2},-\tfrac{3}{2})&=\frac{1}{\sqrt{2}}(\mathbf{X}'-i\mathbf{Y}')\downarrow\,.
\end{aligned}
\tag{5.5}
$$

Although for Γ_8^c and $\mathbf{k}\|[110]$ the eigenstates are not well described by Eqs. (5.4) and (5.5), still one set has predominantly $(\frac{3}{2},\pm\frac{3}{2})$ and the other $(\frac{3}{2},\pm\frac{1}{2})$ character. We shall determine the signs of the splittings by calculating analytically by perturbation theory the splittings for small k

(proportional to k^3). They will be checked by evaluating the y components of the spin in the LMTO calculations below. Agreement is found in all cases.

B. Perturbation expansions of the spin splittings

1. Γ_1 band along [110]

All bands along [110] are split by spin-orbit interaction. We write the splitting for small k as[5,6,9]

$$\Delta E=\gamma k^3 , \tag{5.6}$$

where the sign of γ corresponds to the convention in Sec. V A (positive if the Σ_4 is above the Σ_3 state). We shall use γ with subscripts γ_c, γ_{sh}, γ_{hh}, γ_{lh}, γ_{se}, γ_{le}, and γ_{he} to represent the splittings of the Γ_6 conduction band, and the Γ_8^v,Γ_7^v and Γ_8^c,Γ_7^c bands (see Fig. 6). The γ's can be obtained either by third-order (in $\mathbf{k}\cdot\mathbf{p}$) perturbation theory from states which include exactly Δ_0, Δ_0', and Δ^- or by fourth-order perturbation theory (3 times $\mathbf{k}\cdot\mathbf{p}$ and once $H_{s.o.}$; see Fig. 19) from the orbital states. The former is more accurate since it treats $H_{s.o.}$ to all orders, while the latter would lead to errors if the Δ's are not much smaller than all energy denominators (e.g., for InSb, $\Delta_0=0.8$, $E_0=0.23$). In all expressions given here the Δ_0 splitting [term (a) of Fig. 19] has been treated to all orders.

We first discuss the four terms contributing to γ_c (Fig. 19) which, in atomic units, are

$$\begin{aligned}
\gamma_c&=\mathcal{A}+\mathcal{B}+\mathcal{C}+\mathcal{D} ,\\
\mathcal{A}&=\frac{4}{3}\left[PP'Q\frac{\Delta_0}{3E_0(E_0+\Delta_0)}\left[\frac{1}{(E_0'-E_0+\Delta_0')}+\frac{2}{E_0'-E_0}\right]\right] ,\\
\mathcal{B}&=\frac{4}{3}\left[PP'Q\frac{\Delta_0'}{(E_0'-E_0)(E_0'+\Delta_0'-E_0)}\left[\frac{1}{E_0+\Delta_0}+\frac{2}{E_0}\right]\right] ,\\
\mathcal{C}&=-\frac{4}{3}\frac{P^2Q\Delta^-}{\bar{E}_0^2(\bar{E}_0'-E_0)} ,\\
\mathcal{D}&=-\frac{4}{3}\frac{P'^2Q\Delta^-}{\bar{E}_0(\bar{E}_0'-E_0)^2} ,
\end{aligned} \tag{5.7}$$

where the bar above E_0 and E_0' represents an average of the two spin-orbit-split components with weight two for Γ_7 and one for Γ_8. According to Table I all terms in Eq. (5.7) are additive for GaAs, GaSb, and InSb. For InP, however, since Δ^- is positive, $\mathcal{C}$ and $\mathcal{D}$ subtract from $\mathcal{A}$ and $\mathcal{B}$. The values of the various components of Eqs. (5.7) for InSb obtained with the parameters of Table I are

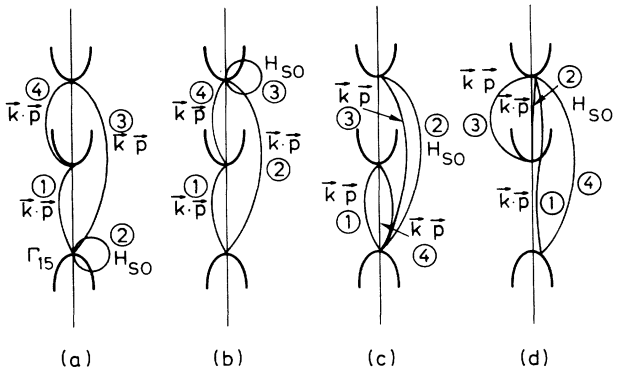

FIG. 19. Diagrams of the four terms which contribute to the coefficient γ of the Γ_{15}^c valence bands [Eq. (5.7)].

$$\begin{aligned}
\gamma_c&=82\ (=\mathcal{A})+6\ (=\mathcal{B})+29\ (=\mathcal{C})+1\ (=\mathcal{D})\\
&=+118\ \text{a.u.} .
\end{aligned} \tag{5.8}$$

In order to convert from atomic units (hartrees bohrs^3) to eV Å^3, one must multiply by 4.05. The values of γ_c obtained with Eq. (5.7) for the four materials discussed here are listed in Table VII, together with values obtained by diagonalization of the full 16×16 $\mathbf{k}\cdot\mathbf{p}$ Hamiltonian and the LMTO values to be discussed below. The results of Eqs. (5.7) are in rather good agreement with those obtained from the full $\mathbf{k}\cdot\mathbf{p}$ Hamiltonian but, in the cases of GaAs and InSb, considerably higher than the LMTO ones. The experimental ones (obtained for GaAs, GaSb, and InP from the Hanle effect[14] and for InSb from electric-field-induced spin resonance[16,18]) agree better with the $\mathbf{k}\cdot\mathbf{p}$ values for the Ga compounds, but with the LMTO values for the In compounds. In the case of InSb the sign has been determined experimentally.[18] It agrees with that found here.

2. Γ_{15}^v bands along [110]

As mentioned above, the Γ_8^v components of these bands are, to a good approximation, symmetry related to the $|j,m_j\rangle=(\frac{3}{2},\pm\frac{3}{2}),(\frac{3}{2},\pm\frac{1}{2})$ angular-momentum functions with the quantization axis along [110], i.e., they can be labeled heavy- and light-hole bands, respectively. A perturbation-theoretical calculation shows that the γ coefficient of the heavy-hole bands (γ_{hh}) is zero. They spin split, however, to orders higher than k^3 (k^5, etc.). The full $\mathbf{k}\cdot\mathbf{p}$ calculations confirm this result. For the light-hole bands perturbation theory yields

$$\gamma_{lh}=\frac{4PP'Q}{3E_0\bar{E}_0'}-\frac{4P^2Q\Delta^-}{3E_0\bar{E}_0'\Delta_0}-\frac{2Q^3\Delta^-}{3E_0'^2\Delta_0} . \tag{5.9}$$

We note that Eq. (5.9) has an energy denominator Δ_0 which can be rather small, especially for InP (~0.1 eV). In these cases Eq. (5.9) may not be a good approximation and terms of higher order in $H_{s.o.}$ may play an important role, even to third order in k. We find the γ's obtained with Eq. (5.9), however, to yield a rather good approximation to the splitting found through diagonalization of

TABLE VII. Values of the coefficient of the spin splitting (Γ_1, Γ_{15}^v, and Γ_{15}^c bands) proportional to k^3 for $\mathbf{k}\|[110]$ as obtained with the LMTO method the 16×16 $\mathbf{k}\cdot\mathbf{p}$ Hamiltonian, and $\mathbf{k}\cdot\mathbf{p}$ perturbation theory (PT) (in hartrees bohrs^3). The signs correspond to the unit-cell convention discussed in the text (anion at origin). For γ_c, experimental data from Refs. 14 (absolute values, GaAs, GaSb, InP) and 18 are also given.

		GaAs	GaSb	InP	InSb	ZnSe	CdTe	CuBr
γ_c	LMTO	+3.7	+27	−2.2	+54	+0.4	+2.9	≈0
	$\mathbf{k}\cdot\mathbf{p}$	+7.0	+38	−2.3	+140			
	$\mathbf{k}\cdot\mathbf{p}$ (PT)	+7.4	+38	−2.9	+118			
	Expt.	6.3	46	2.1	+56			
γ_{lh}	LMTO	+10	+37	−31	+64	+2.1	+5.1	
	$\mathbf{k}\cdot\mathbf{p}$	+28	+64	−28	+168			
	$\mathbf{k}\cdot\mathbf{p}$ (PT)	+29	+64	−41	+190			
γ_{sh}	LMTO	+5.2	+13.6	−25	+12	+1.5	0.0	≈0
	$\mathbf{k}\cdot\mathbf{p}$	+18	+26	−21	+40			
	$\mathbf{k}\cdot\mathbf{p}$ (PT)	+19	+22	−37	+39			
γ_{le}	LMTO	−2.8	+3.6	−3.0	−3.6	−0.3	−1.1	≈0
	$\mathbf{k}\cdot\mathbf{p}$	−2	+7.2	−6.4	−2.2			
	$\mathbf{k}\cdot\mathbf{p}$ (PT)	−4.2	−1.6	−3.7	−4.3			
γ_{he}	LMTO	+0.4	+0.4	−2	+1	−0.1	−0.5	≈0
	$\mathbf{k}\cdot\mathbf{p}$	−1.4	≈0	−3.2	+0.5			
	$\mathbf{k}\cdot\mathbf{p}$ (PT)							
γ_{se}	LMTO	−3.3	−3.6	−4.1	−5.6	−0.6	−2.0	±0.1
	$\mathbf{k}\cdot\mathbf{p}$	−5.4	−4.2	−4.5	−4.0			
	$\mathbf{k}\cdot\mathbf{p}$ (PT)	−5.5	−4.4	−4.4	−6.9			

the complete $\mathbf{k}\cdot\mathbf{p}$ Hamiltonian and graphical evaluation of the k^3 terms (see Table VII).

The γ coefficient of the split-off Γ_{15}^v band [Γ_7^v, $(\frac{1}{2},\pm\frac{1}{2})$], γ_{sh}, is very similar to that of Eq. (5.9). It can be obtained from this equation by replacing E_0 by $E_0+\Delta_0$ and E_0' by $E_0'+\Delta_0'$. The results of the calculation based on this prescription are also compared in Table VII with those obtained from the full $\mathbf{k}\cdot\mathbf{p}$ Hamiltonian and from the LMTO calculations.

3. Γ_{15}^c bands along [110]

The Γ_7^c components correspond for $\mathbf{k}$ along [110] to the $(\frac{1}{2},\pm\frac{1}{2})$ combinations of wave functions, with [110] being the quantization axes. The corresponding γ (γ_{se}) is

$$\gamma_{se}=\frac{4PP'Q}{3(E_0'-E_0)(E_0'+2\Delta_0/3)}+\frac{4(P')^2Q\Delta^-}{3(E_0'-E_0)(E_0'+2\Delta_0/3)\Delta_0'}+\frac{2Q^3\Delta^-}{3(E_0'+2\Delta_0/3)^2\Delta_0'}+\frac{4(P''')^2Q\Delta^-}{3(E_0'''-E_0')(E_0'+2\Delta_0/3)\Delta_0'}\,. \tag{5.10}$$

The sign of the first three terms in γ_{se} is opposite that of γ_{sh} because of a change in the product of matrix elements. The energy denominators change sign with no net effect in the total sign. The fourth term is due to the interaction with the Γ_1' band (the next-higher Γ_1 conduction band).

The expression for γ_{le} is basically the same with Δ_0' added to E_0'. In order to give a feeling for the magnitude and sign of the various contributions to γ_{se} contained in Eq. (5.10), we list them below for GaSb in the order of Eq. (5.10),

$$\gamma_{se}=-8.9-2.6-2.6+9.7$$
$$=-4.4\ \text{a.u.} \tag{5.11}$$

The values calculated in this manner for γ_{se} and γ_{le} for GaAs, GaSb, InP, and InSb are given in Table VII. Because of the fact that the perturbation calculation of γ_{le} has been done under the assumption of pure $(\frac{3}{2},\pm\frac{1}{2})$ states, it is not as reliable as the calculations of γ_{se}. Also, in that case, the full $\mathbf{k}\cdot\mathbf{p}$ calculation should give better results. Similarly, the perturbation calculation of γ_{he} yields zero, while the full calculation does not.

4. Discussion

We find, on the whole, reasonably good agreement between the three theoretical estimates of the γ's listed in Table VII and also, in the case of γ_c, with the experimental values. Particularly satisfactory is the sign agreement. The theoretical signs were determined in the case of the perturbation calculation by careful self-consistent choice of all matrix elements of $\mathbf{p}$ and $H_{s.o.}$ (see above). In the

LMTO calculations we determined the sign of γ by the expectation value of spin along $[1\bar{1}0]$ (with the exception of γ_{he}). It was also possible to determine in this manner the signs of C_k and C_k', the coefficients of the linear terms in k (see below). Once the sign of C_k was known, we were able to determine that of γ_{he} by observing whether the cubic term in k had the same or opposite sign as the linear one. With the signs of C_k and C_k' known, it was trivial to determine those of γ_{le}, γ_{lh}, and γ_{hh} in the full $\mathbf{k}\cdot\mathbf{p}$ calculation. The signs of γ_{se} and γ_{sh} in this case were assumed to be those given by perturbation theory since the magnitudes of the full $\mathbf{k}\cdot\mathbf{p}$ calculations and those of the latter agree (the only exception, γ_{se} for InSb, the discrepancy probably being due to the large value of Δ_0 and the small value of E_0, which may make the perturbation expansion inaccurate).

Let us next discuss γ_c. Experiments based on the Hanle effect[14] measure a lifetime and thus do not give information on the sign of γ_c. Those of Refs. 17 and 18 for InSb measure an interference between two transition matrix elements, one proportional to γ_c and the other of known sign. Hence they yield the sign of γ_c (positive with our convention: anion at the origin of coordinates). This sign agrees with the theoretical one. The magnitudes of γ_c found by the different methods are mostly in acceptable agreement with each other, the possible exception being InSb, where the LMTO result agrees extremely well will experiment, the $\mathbf{k}\cdot\mathbf{p}$ data being a factor of 2–3 too high. The LMTO calculations can be regarded as *ab initio* and thus include all states of s, p, and d symmetry, particularly the core levels. One may therefore take them more seriously than the others. They have, nevertheless, two handicaps: the gap adjustments [Eq. (3.1) and Table IV] and the spherical charge symmetrization in each of the spheres. The gap adjustments change the γ's in the manner suggested by Eqs. (5.7), (5.9), and (5.10), if one changes only the energy denominators. It is thus reasonable to assume that they lead to correct values of γ. The error introduced by the charge symmetrization is more difficult to estimate, but should be small. The fully relativistic nature of the LMTO calculations may also lead to improved results with respect to the $\mathbf{k}\cdot\mathbf{p}$ data, especially in the case of materials with heavy atoms such as InSb. The agreement among all values of γ_c is rather good for InP and InSb. For GaAs the LMTO data lead also to values nearly half of those obtained with $\mathbf{k}\cdot\mathbf{p}$. The experimental results, however, fall closer to the LMTO calculation for InSb and closer to the $\mathbf{k}\cdot\mathbf{p}$ results for GaAs and GaSb. The contributions of the four terms of Eq. (5.7) for InSb are given in Eq. (5.8). Those for GaAs are

$$4.0\ (=\mathcal{A})+1.1\ (=\mathcal{B})+2.1\ (=\mathcal{C})+0.2\ (=\mathcal{D})=7.4\ . \tag{5.12}$$

In the case of InSb, agreement of the γ_c estimated using Eq. (5.7) with the other three γ_c values would be restored by inverting the sign of Δ^- (change in sign of terms $\mathcal{C}$ and $\mathcal{D}$, $\gamma=+58$). Nevertheless, this would lead to the wrong sign for the contribution of Δ^- to the g factor.[36,37] A reversal of Δ^- in InSb would most likely also imply a reversal in Δ^- for InP and GaAs. This would lead in the former materials to the wrong sign of γ_c (as compared with LMTO), in the latter to $\gamma_c=2.8$, considerably smaller than the experimental value. At present, we must leave the question of the origin of the discrepancy open since no obvious pattern is discernible in it. Calculations for more materials may help.

For the other γ's in Table VII no experimental data exist that would help us sort out other existing discrepancies between LMTO and $\mathbf{k}\cdot\mathbf{p}$ data (however, recent spin-polarization measurements for InP and GaSb are consistent with the γ_{sh}'s given in Table VII; see Ref. 15). For γ_{sh} and γ_{lh} the LMTO values also tend to be smaller than the $\mathbf{k}\cdot\mathbf{p}$ ones, with the exception of InP.

In the case of the Γ_{15}^c bands the $\mathbf{k}\cdot\mathbf{p}$ values of γ_{se} agree rather well with those calculated by means of the LMTO method. We should point out, however, that in order to obtain this agreement it is of the essence to include the upper Γ_1' conduction-band state, particularly its coupling to Γ_{15}^c via P'''. In the case of γ_{le}, one should only compare the results of the full $\mathbf{k}\cdot\mathbf{p}$ calculation since those of perturbation theory suffer from the incorrectness of the $(\frac{3}{2},\pm\frac{1}{2})$ ansatz. There is agreement in the sign of γ_{le} between $\mathbf{k}\cdot\mathbf{p}$ and LMTO values and their magnitudes agree fairly well, especially when one considers that these states are rather high in energy and thus may interact with higher states that have not been included in the $\mathbf{k}\cdot\mathbf{p}$ Hamiltonian.

For the II-VI compounds ZnSe and CdTe and for the I-VII compound CuBr we only have LMTO results. The strong drop in the γ's in these compounds as compared to the corresponding isoelectronic III-V compounds (GaAs→ZnSe→CuBr) is rather striking. The most likely explanation lies in the influence of the d core levels of the cation [binding energies with respect to Γ_{15}^v: GaAs, 18.8 eV; ZnSe, 9.2 eV; CuBr, 2 eV (Ref. 10)]. This suggests that the d core levels of the III-V compounds, not included in the $\mathbf{k}\cdot\mathbf{p}$ calculation, may also contribute to the discrepancy between $\mathbf{k}\cdot\mathbf{p}$ and LMTO results.

VI. STRAIN-INDUCED LINEAR TERMS IN $\mathbf{k}$

Upon application of linear strain, the symmetry of the crystal is lowered and spin splittings linear in k may result from the combined effect of the $\mathbf{k}\cdot\mathbf{p}$ and the strain Hamiltonian.[54] One may regard them as the result of replacing two powers of k in γk^3 by a symmetry-equivalent strain. Such terms also appear, for the same reasons, in crystals with wurtzite structure even without strain.[55] They have been observed for the Γ_1 bands of InSb by means of Shubnikov–de Haas measurements[56] and in its valence band by means of cyclotron resonance.[57] Linear terms in the Γ_6 conduction band appear through the coupling via the strain Hamiltonian of this band with the Γ_{15}^c and Γ_{15}^v bands. This coupling can only be effected through a strain of Γ_{15} symmetry, i.e., through the ϵ_{ij} $(i\neq j)$ components of the strain. This coupling is characterized by parameters referred to in the literature as $d^{v,cs}$, $d^{c,cs}$ or $C_2=2d^{v,s}$.[31] They are defined as[31]

$$d^{v,cs}=\langle \Gamma_1 \mid H(\epsilon_{xy}) \mid \Gamma^v_{15,z} \rangle \ ,$$
$$d^{c,cs}=\langle \Gamma_1 \mid H(\epsilon_{xy}) \mid \Gamma^c_{15,z} \rangle \ . \tag{6.1}$$

The values of these parameters calculated with the pseudopotential and the LCAO method[31] are listed in Table VIII for GaAs, GaSb, InP, and InSb. The Γ^c_{15} and Γ^v_{15} are coupled by strains of Γ_{15} (i.e., compression along [111]) and Γ_{12} (along [100]) symmetry. The corresponding deformation potentials, which are also given in Ref. 31, affect the spin splittings linear in strain and k of the Γ^c_{15} and Γ^v_{15} bands. For a [100] strain they are the determining factor. Experimental data for these bands are only available for InSb.[57] We shall not discuss this point any further.

We write the spin splitting induced by the $\epsilon_{xy}=\epsilon_{yx}$ components of the strain for $\mathbf{k}\|[110]$ as[58,20]

$$\Delta E(\Sigma_4-\Sigma_3)=V_2 k \epsilon_{xy} \ , \tag{6.2}$$

where the symmetries Σ_4 and Σ_3 refer to the [110] reflection plane. Using second-order perturbation theory, we find

$$V_2=\frac{8}{3}\left[-\frac{d^{v,cs}P\Delta_0}{E_0(E_0+\Delta_0)}-\frac{d^{c,cs}P'\Delta'_0}{(E'_0-E_0)(E'_0-E_0+\Delta'_0)}\right.$$
$$\left.+\frac{(d^{v,cs}P'+d^{c,cs}P)\Delta^-}{(E_0+2\Delta_0/3)(E'_0-E_0+2\Delta'_0/3)}\right] . \tag{6.3}$$

The values of V_2 obtained with Eq. (6.3) for the parameters of Table I and the two sets of deformation potentials of Table VIII are given in Table IX and compared with experimental data. The latter fall for GaAs and GaSb close to the pseudopotential value, while in the case of InP it is closer to the LCAO result. The experimental result for InSb were reconstructed from the Shubnikov–de Haas measurements of Seiler *et al.*[56] by using their values of P, E_0, Δ_0, and $d^{v,cs}=C_2/2$ and no other contributions than the Γ_1-Γ^v_{15} interaction. It is somewhat smaller than the theoretical one, a fact which is also reflected by the value of $d^{v,cs}=C_2$ obtained by these authors (see Table VIII).

TABLE VIII. Interband deformation potentials (in eV) of four III-V semiconductors calculated with the pseudopotential (ps) and LCAO method (Ref. 31). For the latter we list the average of values obtained with sp^3 and sp^3s^* bases. For the calculation, the internal strain parameter ζ has been assumed to be 0.7. Experimental values of $d^{v,cs}$ equal to 1 and 1.5 eV have been reported for InSb.

		GaAs	GaSb	InP	InSb
$d^{v,cs}$	ps	0.55	0.69	1.1	1.24
	LCAO	2.75	2.2	2.6	2.25
$d^{c,cs}$	ps	2.8	2.6	1.9	2.1
	LCAO	3.0	2.9	2.35	2.2

TABLE IX. Parameter V_2 which, according to Eq. (6.2), determines the spin splitting of the Γ_1 bands linear in strain and k (in a.u.). Values calculated from the pseudopotential (ps) and LCAO deformation potentials with Eq. (6.3) are given. The magnitudes of the experimental values are also given.

		GaAs	GaSb	InP	InSb
V_2	ps	−0.26	−1.2	−0.03	−7.6
	LCAO	−0.78	−2.9	−0.11	−13.6
	Expt.[a]	0.27[b]	1.0[b]	0.11–0.21[b]	5.5[c]

[a]Absolute value.
[b]Reference 14.
[c]Reference 57.

VII. TERMS LINEAR IN k

The reader will have already noticed the terms linear in the components of $\mathbf{k}$, with coefficients C_k in the Hamiltonian of the Appendix. They result in spin splittings linear in k for the $(\frac{3}{2},\pm\frac{3}{2})$ and $(\frac{3}{2},\pm\frac{1}{2})$ Γ^v_8 bands when $\mathbf{k}$ is along $\langle 110\rangle$ and for the $(\frac{3}{2},\pm\frac{3}{2})$ bands only for $\mathbf{k}$ along $\langle 111\rangle$. This splitting does not arise for $\mathbf{k}$ along $\langle 100\rangle$. Similar terms have been included for the Γ^c_8 bands in our $\mathbf{k}\cdot\mathbf{p}$ Hamiltonian. We designated the corresponding coefficient by C'_k. Two different contributions to C_k (and C'_k) have been identified. One of them arises from operating with $H_{\text{s.o.}}$ on the Bloch function $\psi_{\mathbf{k}}=u_{\mathbf{k}}e^{i\mathbf{k}\cdot\mathbf{r}}$ and treating one of the terms in first-order perturbation theory:[5,6]

$$C^a_k=-\frac{1}{2\sqrt{3}c^2}\left\langle \Gamma_{15,x}\left|\frac{\partial V}{\partial y}\right|\Gamma_{15,z}\right\rangle . \tag{7.1}$$

The others arise in second-order perturbation theory, taking one matrix element of $\mathbf{k}\cdot\mathbf{p}$ and one of $H_{\text{s.o.}}$. The only allowed intermediate states for these terms have Γ_{12} (C^b_k) and Γ_{25} (C^c_k) symmetries,[5,6] and thus they have not been included in our basis, nor has C^a_k. This is why they have to be represented in Eq. (A2) by additional parameters C_k and C'_k.

Despite early estimates,[5,6] it is easy to show that C^a_k can be neglected.[59] Let us consider the commutator

$$[p_y,H]=-i\frac{\partial V}{\partial y} \tag{7.2}$$

and take its matrix elements between the $\Gamma_{15,x}$ and $\Gamma_{15,z}$ states:

$$\left\langle \Gamma_{15,x} \left| \frac{\partial V}{\partial y} \right| \Gamma_{15,z} \right\rangle = i\langle \Gamma_{15,x} | [p_y, H] | \Gamma_{15,z} \rangle = iE(\Gamma_{15})\langle \Gamma_{15,x} | p_y - p_y | \Gamma_{15,z} \rangle = 0 \ . \tag{7.3}$$

We may also conjecture that the C_k^c contribution is negligible. The corresponding intermediate states have Γ_{25} symmetry, which corresponds to atomic orbitals of angular momentum 3 (f-like) or higher. Such orbitals are not available in the cores of the materials considered here. The empty states of such symmetry are very high and should have negligible spin-orbit coupling to the Γ_{15} states. In any case, f states have not been included in the LMTO calculation. Hence we conclude that the main contribution to the C_k's comes from the bilinear terms consisting of $\mathbf{k}\cdot\mathbf{p}$ and $H_{\text{s.o.}}$ as perturbations, with Γ_{12}-like intermediate states. Because of the large spin-orbit splittings involved, we conjecture that these intermediate states are the outermost d-like core levels of the two constituent atoms.

A. Splitting along [111]

We show in Fig. 20 the splittings of the heavy-hole Γ_8^v bands $(\frac{3}{2},\pm\frac{3}{2})$ of GaAs, GaSb, InP, InSb, ZnSe, and CdTe as obtained with the LMTO method for $\mathbf{k}\|[111]$. The corresponding splitting for CuBr is much larger and can be read off directly from Fig. 16. Figure 21 displays similar results for the "heavy-electron" Γ_8^c bands. We note that for small k the splittings are linear in k. Here, however, k has always been kept sufficiently large so as to have the k^2 splitting between the heavy and light carrier bands (due to the effective mass difference) much larger than the spin splitting. For very small values of k the C_k terms will couple $(\frac{3}{2},\pm\frac{1}{2})$ with $(\frac{3}{2},\pm\frac{3}{2})$ and nonlinearities will arise. We have not investigated this region; it can be done easily and reliably with the $\mathbf{k}\cdot\mathbf{p}$ Hamiltonian.

In the linear region of Figs. 20 and 21 the eigenstates of the split bands are similar to those given in Eq. (5.5), but with the quantization axis $\hat{\mathbf{z}}$ replaced by [111]. Their symmetries are Λ_4 (compatible with Σ_3), Λ_5 (compatible with Λ_4) and Λ_6 (doubly degenerate, compatible with $\Sigma_3+\Sigma_4$). In the figures we have plotted $E(\Lambda_5)-E(\Lambda_4)$ (with the signs given near each curve). The linear splitting is related to the C_k's via[5,6]

$$E(\Lambda_5)-E(\Lambda_4) = -2\sqrt{2}C_k k \ . \tag{7.4}$$

We have determined the values of C_k and C_k' from the slopes of Figs. 20 and 21 for small k. They are listed in Tables X and XI. The signs of these parameters were determined through the interference with the cubic splitting (γ's) calculated for $\mathbf{k}\|[110]$ (see Sec. VII B). Note in Fig. 20 that all splittings are sublinear in k with increasing k, with the exception of GaSb, for which a supralinear increase is found. This supralinearity seems to be related to the fact that C_k is positive for GaSb and negative for the other materials. Note that a similar phenomenon occurs for the Γ_8^c bands (Fig. 21): the spin splitting is supralinear for InP ($C_k<0$) and sublinear for

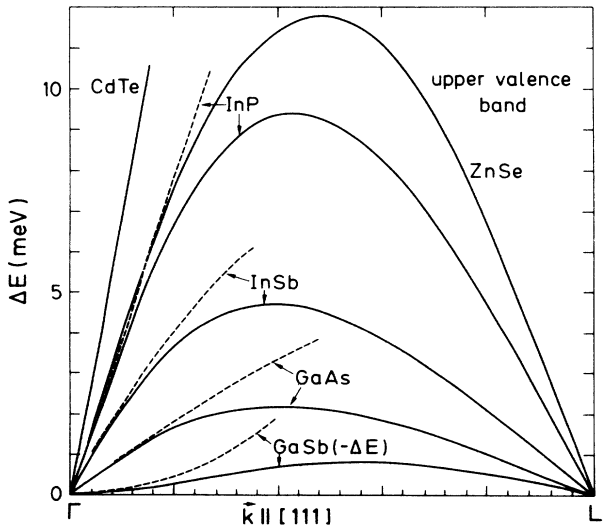

FIG. 20. Spin splittings of the upper valence band (heavy hole) of GaAs, GaSb, InP, InSb, ZnSe, and CdTe calculated with the LMTO method. The dashed lines represent the results of the parametrized $\mathbf{k}\cdot\mathbf{p}$ calculations.

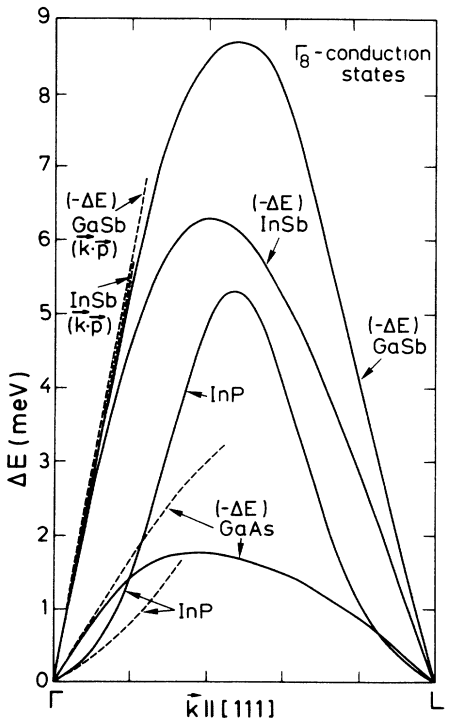

FIG. 21. Spin splittings of the upper heavy-electron Γ_8-conduction band of GaAs, GaSb, InP, and InSb along [111] calculated with the LMTO method. The dashed lines represent the results of the parametrized $\mathbf{k}\cdot\mathbf{p}$ calculations.

TABLE X. Values of the parameters required for the calculations of C_k with Eq. (7.6) and calculated C_k's (in meV Å) compared with the results obtained with the LMTO method and with available experimental data.

Material	$\Delta_{d,c}$	$\Delta_{d,a}$	$E(\Gamma_8)-E_{d,c}$	$E(\Gamma_8)-E_{d,a}$	C_k(LMTO) $\mathbf{k}\|\|[111]$	C_k(LMTO) $\mathbf{k}\|\|[110]$	C_k [Eq. (7.6)]	$\|C_k\|$ (Expt.)
AlAs	0	0.53		40.95[a]			+2.0	
AlSb	0	1.25		32.2[b]			+6.0	
GaP	0.36	0	18.7[c]				−5.5	
GaAs	0.36	0.53	18.85[d]	40.8[e]	−3.4	−3.6	−3.4	
GaSb	0.36	1.25	18.95[d]	31.75[e]	+0.4	+0.7	+0.7	
InP	0.88	0	17.4[d]		−13.7	−14.4	−14.4	
InAs	0.88	0.53	17.2[d]	40.65[e]	−9.5	−9.2	−11.2	
InSb	0.88	1.25	17.4[d]	31.35[e]			−8.2	9.3[j]
ZnS	0.4[f]	0	9.03[c]				−15.5	
ZnSe	0.4[f]	0.83	9.2[f,g]	53.35[g]	−14.5	−14.1	−13.8	12[k]
ZnTe	0.4[f]	1.51	9.6[h]	40.0[h]			−11.2	<10[l]
CdTe	0.79[f]	1.51	10.3[h]	40.2[h]	−27.0	p	−23.4	20.6[m]
HgSe	1.8	0.83	7.93[h]	53.4[h]			−80.2	
HgTe	1.85[h]	1.51	8.3[h]	39.7[h]			−74.6	
CuCl	0.34[f]	0	1.8[i]				−78	82[q]
CuBr	0.34[f]	1.0	2.0[i]	70	−86.0	p	−70	73,[n] 50[o], 69[q]
CuI	0.34[f]	1.87[f]	2.1[i]	50			−66	36[q]
AgI	0.48[f]	1.87[f]	4[i]	50			−48	

[a]Estimated from the values of GaAs and InAs.
[b]N. J. Shevchik, J. Tejeda, C. M. Penchina, and M. Cardona, Solid State Commun. **11**, 1619 (1972).
[c]L. Ley, R. A. Pollak, F. R. McFeeley, S. P. Kowalczyk, and D. A. Shirley, Phys. Rev. B **9**, 600 (1974).
[d]Reference 17.
[e]W. Gudat, E. E. Koch, P. Y. Yu, M. Cardona, and C. M. Penchina, Phys. Status Solidi B **52**, 505 (1972).
[f]F. Herman and S. Skillman, *Atomic Energy Levels* (Prentice-Hall, Englewood Cliffs, NJ, 1963).
[g]N. J. Shevchik, J. Tejeda, D. Langer, and M. Cardona, Phys. Status Solidi B **60**, 345 (1973).
[h]N. J. Shevchik, J. Tejeda, M. Cardona, and D. Langer, Phys. Status Solidi B **59**, 87 (1973).
[i]S. Ves, D. Glötzel, M. Cardona, and H. Overhof, Phys. Rev. B **24**, 3073 (1981); N. E. Christensen, Int. J. Quantum Chem. **XXV**, 233 (1984); A. Goldmann, J. Tejeda, and M. Cardona, Phys. Rev. B **10**, 4388 (1974).
[j] *Landoldt-Börnstein Tables,* edited by O. Madelung, M. Schultz, and H. Weiss (Springer, Berlin, 1982), Vol. 17a; see also Ref. 3.
[k]Reference 7.
[l]Reference 6.
[m]Reference 5.
[n]Reference 4.
[o]D. P. Vu, Y. Oka, and M. Cardona, Phys. Rev. B **24**, 765 (1981).
[p]No values are listed since the 3:1 rule is not obeyed. See text.
[q]T. Itoh, Y. Iwabuchi, and T. Kirihara, Phys. Status Solidi B (to be published).

all other materials ($C_k > 0$).

We have also plotted in Figs. 20 and 21 the spin splittings obtained for our 16×16 $\mathbf{k}\cdot\mathbf{p}$ Hamiltonian (dashed lines). The linear regions for small k agree with the LMTO results by construction. The LMTO trends of the deviation from linearity are also reproduced by the $\mathbf{k}\cdot\mathbf{p}$ calculation, although quantitative differences exist.

B. Splittings along [110]

We show in Figs. 22–27 the spin splitting found for the Γ_{15}^{v} and Γ_1 bands for six of the compounds under consideration with the LMTO method [similar curves are not shown for CuBr, due to the ambiguity; cf. Figs. 14(a)

TABLE XI. Values of C_k' (in meV Å), the coefficient of spin splittings linear in k of the Γ_8 conduction bands, calculated with the LMTO method for $\mathbf{k}\|[111]$ (correct values) and for $\mathbf{k}\|[110]$ [incorrect due to $(\frac{3}{2},\pm\frac{3}{2})$-$(\frac{3}{2},\pm\frac{1}{2})$ admixture]. Also, values calculated with the semiempirical equation (7.8).

C_k'	[111]	$[110]_{he}$	$[110]_{le}$	Eq. (7.8)
GaAs	+3.04	+1.92	+6.43	+3.9
GaSb	+11.3	+7.60	+21.6	+11.7
InP	−1.18	−0.58	−1.74	0
InSb	+11.4	+7.64	+23.6	+11.8
ZnSe	+3.63	2.32	12.1	+3.63
CdTe	+14.8	+6.5	39.0	+14.8
CuBr	+5.72	+3.3	+16.9	+5.7

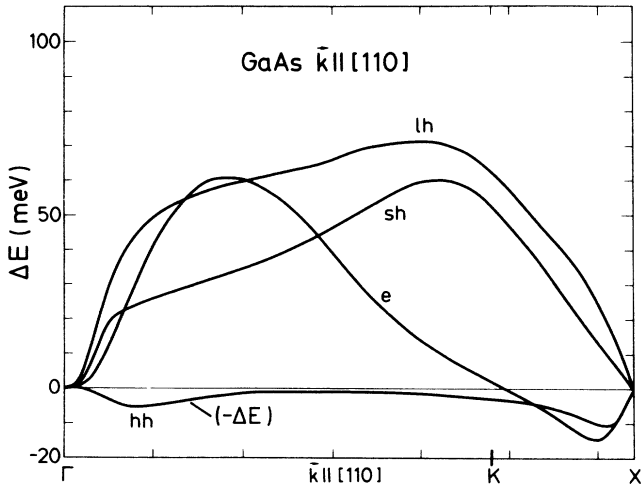

FIG. 22. Spin splittings of the lowest conduction band and the three highest valence bands of GaAs for **k** along [110] as calculated with the LMTO method. The hh splitting is shown for k close to 0 in Fig. 28.

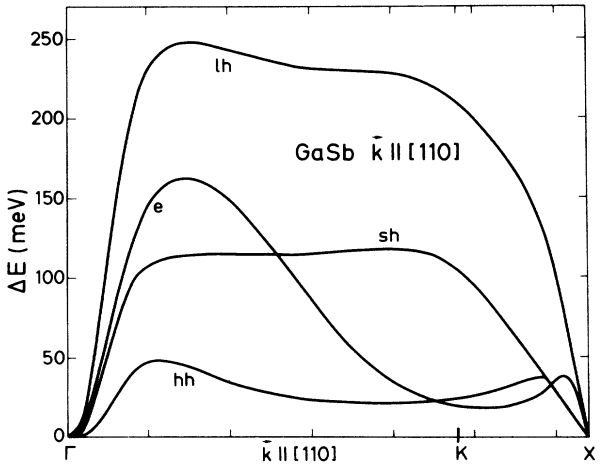

FIG. 23. Spin splittings of the lowest conduction band and the three highest valence bands of GaSb for **k** along [110] as calculated with the LMTO method. The region very close to Γ is shown in Fig. 29.

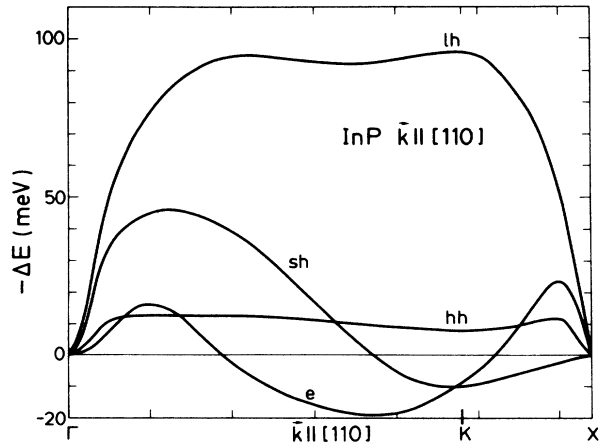

FIG. 24. Spin splittings of the lowest conduction band and the three highest valence bands of InP for **k** along [110] as calculated with the LMTO method. The region very close to Γ is shown expanded in Fig. 31.

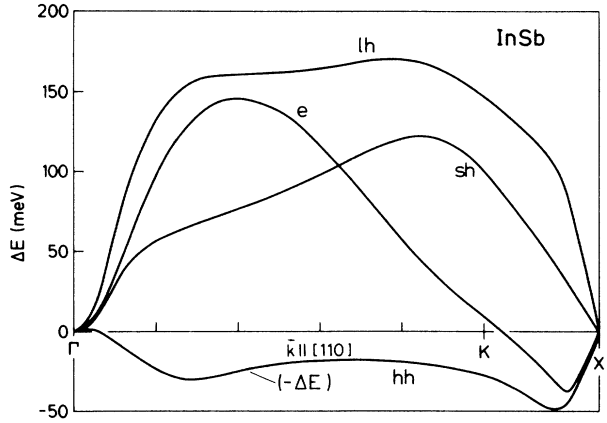

FIG. 25. Spin splittings of the lowest conduction band and the three highest valence bands of InSb for **k** along [110] as calculated with the LMTO method.

and 14(b), in identifying the splittings because of the band crossings]. These splittings are much larger than those of Figs. 20 and 21 since now we not only have the effect of C_k but also the effect of γ and similar higher-order terms in k. The effects of C_k are only of importance for small values of k and can hardly be seen in these figures. For this reason, we show expanded plots of the splittings of the hh band in GaAs in Fig. 28, the hh, lh, sh, and e bands of GaSb in Fig. 29, the Γ_8^c bands in GaSb in Fig. 30, and Γ_8^v and Γ_6^c in InP in Fig. 31. The k-linear terms can be seen in these figures for small k in the splittings of the lh, le, hh, and he bands (Γ_8). The linear term in the hh splitting in GaAs is negative, whereas γ_{hh} is positive. This causes $\Delta E(k)$ to change sign, as seen in Fig. 28, for $k \cong 12.8 d_{\Gamma K}/300$. In GaSb (Fig. 29), C_k is seen to be positive (0.7 meV Å), and also γ_{hh} is positive. Thus, a crossover close to Γ as found in GaAs does not occur in this case. In Fig. 30 the linear term for the le band has a sign opposite that of the cubic term. Since $\gamma_{le} > 0$ (positive Σ_4-Σ_3 splitting, see Table VII) and $C_k > 0$, we con-

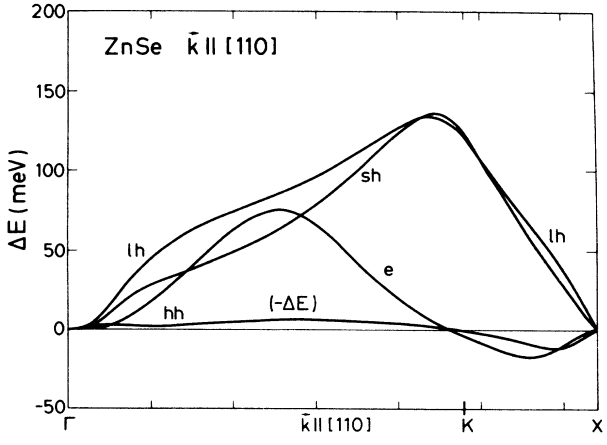

FIG. 26. Spin splittings of the lowest conduction band and the three highest valence bands of ZnSe for **k** along [110] as calculated with the LMTO method.

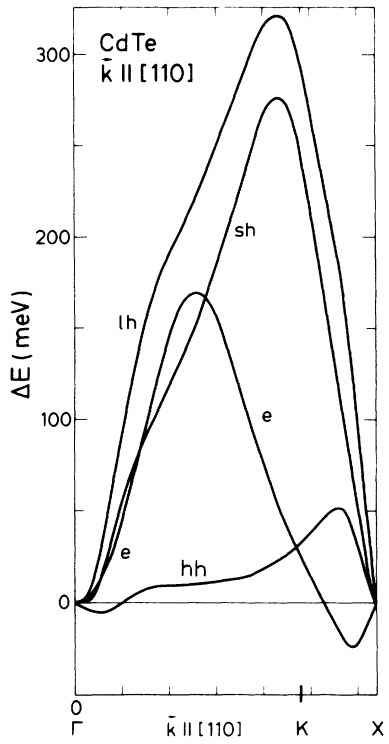

FIG. 27. Spin splittings of the lowest conduction band and the three highest valence bands of CdTe for **k** along [110] as calculated with the LMTO method.

clude that $C_k > 0$ corresponds to a negative Σ_4-Σ_3 splitting in the linear-k region. Similar reasoning leads in Fig. 31 to $\gamma_{lh} < 0$, $C_k < 0$. We note in Fig. 30 that the linear splitting of the lh band is about one-third that of the hh one. This is a consequence of the nearly isotropic nature of the valence bands (see Sec. V A). If we assume that the

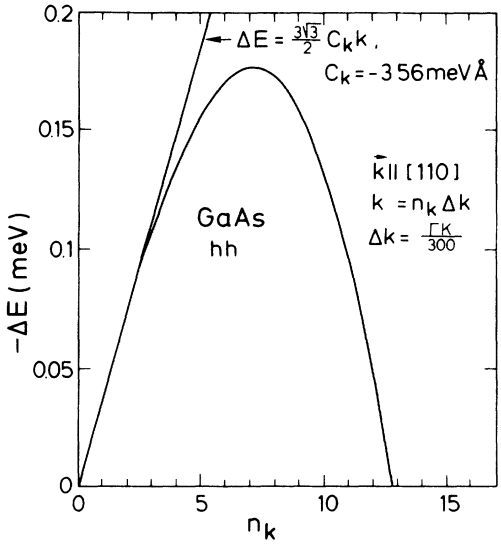

FIG. 28. Splitting of the heavy-hole (hh) band in GaAs for **k**||[110] in the region close to Γ. Note that $-\Delta E$, where $\Delta E \equiv E(\Sigma_4) - E(\Sigma_3)$, is plotted, that C_k (defined from the slope at Γ) is negative, and γ, the third-order coefficient, is positive.

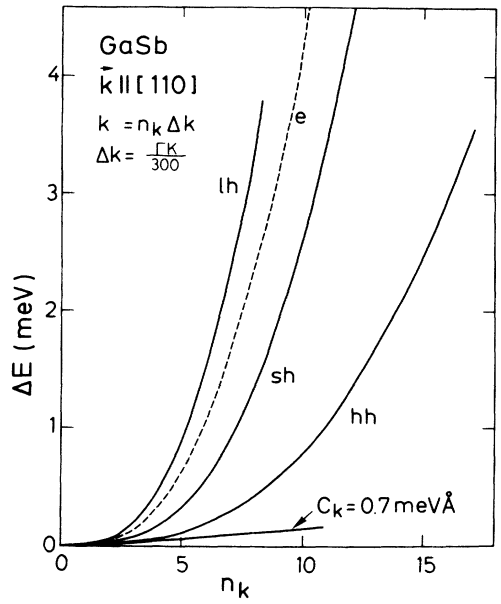

FIG. 29. Detail of the splitting of the uppermost valence bands and the lowest conduction band in GaSb for **k**||[110]. The straight line defines the slope of the hh curve at Γ.

lh and hh functions have symmetries $(\frac{3}{2}, \pm\frac{1}{2})$ and $(\frac{3}{2}, \pm\frac{3}{2})$, we calculate, in the region of a quadratic (effective-mass) splitting larger than the linear one,[5,6]

$$E_{hh}(\Sigma_4) - E_{hh}(\Sigma_3) = +\frac{3\sqrt{3}}{2} C_k k \ ,$$
$$E_{lh}(\Sigma_4) - E_{lh}(\Sigma_3) = -\frac{\sqrt{3}}{2} C_k k \ . \tag{7.5}$$

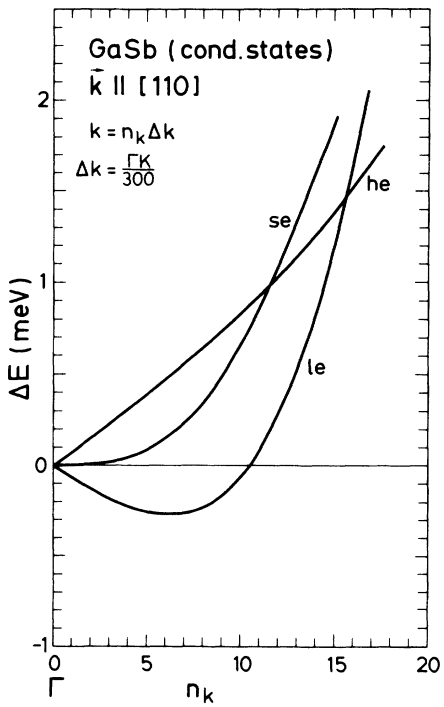

FIG. 30. Detail of the spin splitting of the Γ_8^c band of GaSb for small k's along [110] as calculated with the LMTO method.

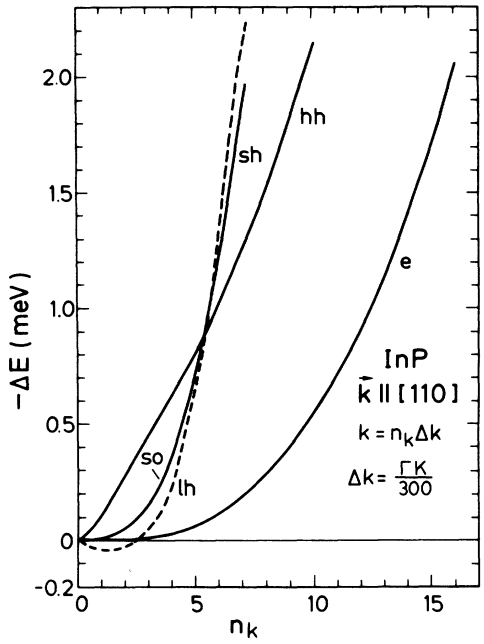

FIG. 31. Detail of the spin splittings of the Γ_8^v and Γ_6^c bands of InP for small k's along [110] as calculated with the LMTO method (see also Fig. 24).

The 3:1 relationship between the splittings of Eq. (7.5) is not fulfilled for the Γ_8^c bands: in Fig. 30 it is rather 1:1. This fact reflects the nonspherical nature of the Γ_8^c bands.

We have also listed in Table X the values of C_k obtained from the linear portion of the hh splittings along [110]. Small discrepancies with the values found from the [111] splittings are due to round-off errors and inaccuracies in reading the computer plots and extracting their slopes. In Table XI we have listed the values of C_k' obtained from the Γ_8^c $(\frac{3}{2},\pm\frac{3}{2})$ splittings for $\mathbf{k}\|[111]$. We have also given the values obtained for $\mathbf{k}\|[110]$ under the incorrect assumption of a pure $(\frac{3}{2},\pm\frac{3}{2})$ and $(\frac{3}{2},\pm\frac{1}{2})$ wave function implicit in Eqs. (7.5) (or their equivalent under the replacements $C_k\rightarrow C_k'$, $h\rightarrow e$). We note that the values obtained from the alleged he $(\frac{3}{2},\pm\frac{3}{2})$ and le $(\frac{3}{2},\pm\frac{1}{2})$ bands do not coincide: the former falls below the correct value (for $\mathbf{k}\|[111]$) while the latter falls above. For the Γ_8^v bands these three values coincided within computational error bars. This fact illustrates the strong deviation from spherical symmetry of the Γ_8^c states.

C. Origin of C_k

We have already mentioned that C_k is mainly produced by bilinear second-order perturbation terms, including $H_{\mathbf{k}\cdot\mathbf{p}}$ and $H_{\text{s.o.}}$, with mainly the outermost core d levels as intermediate states. Thus the following interpolation formula was suggested in Ref. 10:

$$C_k=-A\frac{\Delta_{d,c}}{E(\Gamma_8^v)-E_{d,c}}+B\frac{\Delta_{d,a}}{E(\Gamma_8^v)-E_{d,a}}\ , \tag{7.6}$$

where $\Delta_{d,c}$ and $\Delta_{d,a}$ are the spin-orbit splittings of the outermost cation and anion d levels and $E_{d,c}$, $E_{d,a}$ their energies, respectively. The constants A and B are assumed to be the same for all III-V compounds. They can thus be determined from two of the LMTO values of C_k and then used to estimate C_k for all other III-V compounds using Eq. (7.6) and the parameters of Table X. We used for this procedure the C_k's obtained from LMTO data for $\mathbf{k}\|[110]$ for InP and GaSb and found $A=285$ meV Å and $B=155$ meV Å. Taking into consideration the fact that A should be equal to B for group-IV materials, we estimate in this case $A=B=220$ meV Å as an average of the values found above for the III-V compounds. It is now an easy matter to extrapolate linearly and find for the II-VI compounds $A=350$ meV Å, $B=9$ meV Å, and for the I-VII compounds $A=415$ meV Å, $B=25$ meV Å. The values of C_k evaluated by this procedure are listed under C_k [Eq. (7.6)] in Table X. They agree rather well in magnitude with the few experimental data available (no experimental information on the sign of C_k is available).

It is also possible to estimate A and B directly from band-structure data. For A we can write, e.g.,[10]

$$A=\tfrac{4}{5}\sqrt{3}s\beta(\text{a.u.})\ , \tag{7.7}$$

where β is the admixture of d core wave function in Γ_8 and s the matrix element of p_x between $\Gamma_{15,x}^v$ and the Γ_{12} component of the core levels. Taking from the LMTO calculations $\beta\cong 0.26$ and from optical data[60] $s\approx 0.1$ bohrs^{-1}, we find with Eq. (7.7) for a typical III-V compound $A=3.6\times10^{-2}$ a.u. $=520$ meV Å. This result is in reasonable agreement with the one determined above in view of the rough values of the parameters used. In particular, $\beta=0.26$ represents the *total* d-like component of Γ_8^v, i.e., an upper limit of the core contribution.

It is not as easy to systematize the values calculated for C_k' (Table XI). Maybe the most telling fact is the *negative* sign for InP, while the signs are *positive* in all other cases. The particular feature of InP is the lack of core d levels in the anion. Hence one may conjecture that the strong *positive* values of C_k' due to these levels. We have tried several schemes to describe C_k' in a unified manner and found them not to be fully satisfactory. Hence we present here the *simplest* of them:

$$C_k'=+330\frac{\Delta_{d,a}}{E(\Gamma_8^c)-E_{d,a}}\ \text{meV Å}\ , \tag{7.8}$$

which implies only a contribution of the d levels of the anion cores to C_k'. The *small* negative value of C_k' for InP would, within this scheme, be due to yet unidentified contributions of other states, such as, for instance, the d levels of the cation. If the latter is true, however, it would be difficult to explain why C_k' is larger in InSb than in GaSb. Higher states may also play a role, although their s.o. splitting should be small. Unfortunately, no experimental data which would help to solve this problem are available.

VIII. CONCLUSIONS

We have calculated several effects of spin-orbit coupling and inversion asymmetry in zinc-blende-type semiconductors. These effects have been evaluated by means of *ab initio* LMTO band-structure calculations and with a semiempirical parametrized 16×16 $\mathbf{k}\cdot\mathbf{p}$ Hamiltonian. Emphasis has been put on an unambiguous determination of the signs of the splittings. Three types of effects have been considered in detail: splittings proportional to k^3 for $\mathbf{k}$ along [110], linear in k for $\mathbf{k}$ along [110] and [111], and the spin-orbit coupling between the Γ_{15}^c and Γ_{15}^v bands. Also, strain-induced splittings linear in k have been calculated. In all cases where experimental data are available, our calculations agree with them in magnitude and sign.

Particularly novel in our work is the identification of the interactions responsible for the coefficients C_k and C_k' which determine the splittings linear in k of Γ_8^v and Γ_8^c. They involve the outermost core levels as intermediate states.

ACKNOWLEDGMENTS

We would like to thank U. Rössler, H. Sigg, and W. Zawadzki for a number of illuminating discussions, and S. Gopalan for a critical reading of the manuscript.

APPENDIX: $\mathbf{k}\cdot\mathbf{p}$ HAMILTONIAN

We show in Fig. 1 the convention used for the phases of the orbital wave functions which are taken to be real. Within this convention, and the definition of Eq. (2.1), P, P', and Q are positive. The sign of P''' is irrelevant by construction. The convention also defines the sign of Δ^- as given in Table VI.

Our 16×16 $\mathbf{k}\cdot\mathbf{p}$ Hamiltonian involves matrix elements between the six Γ_{15}^c, six Γ_{15}^v, two Γ_1, and two Γ_1' wave functions. We take as basis the linear combinations of these wave functions times spin which correspond to $(\frac{1}{2},\pm\frac{1}{2}),(\frac{3}{2},\pm\frac{1}{2})$ angular-momentum states, with $\hat{\mathbf{z}}$ (i.e., [001]) as the quantization axis. A portion of this Hamiltonian, namely that between the Γ_7^c,Γ_8^c and the $\Gamma_7^v,\Gamma_8^v,\Gamma_6$ states, is shown in Table I of Ref. 25. In it one must include the coupling through Δ^-, which was omitted in Ref. 25:

$$\langle(\tfrac{1}{2},\tfrac{1}{2})_v\,|\,H_{\text{s.o.}}\,|\,(\tfrac{1}{2},\tfrac{1}{2})_c\rangle=-\tfrac{2}{3}i\Delta^-\ ,$$
$$\langle(\tfrac{3}{2},\tfrac{3}{2})_v\,|\,H_{\text{s.o.}}\,|\,(\tfrac{3}{2},\tfrac{3}{2})_c\rangle=\tfrac{1}{3}i\Delta^-\ , \tag{A1}$$

$$\begin{array}{cccccc}
(\frac{3}{2},\frac{3}{2})_v & (\frac{3}{2},\frac{1}{2})_v & (\frac{3}{2},-\frac{1}{2})_v & (\frac{3}{2},-\frac{3}{2})_v & (\frac{1}{2},\frac{1}{2})_v & (\frac{1}{2},-\frac{1}{2})_v \\
-\frac{1}{2}[\gamma_1'k^2 & \sqrt{3}\gamma_3'k_zk_+ & \frac{\sqrt{3}}{2}\gamma_2'(k_x^2-k_y^2) & -\frac{C_k\sqrt{3}}{2}(k_x-ik_y) & -\sqrt{3/2}\gamma_3'k_zk_+ & -\sqrt{3/2}\gamma_2'(k_x^2-k_y^2) \\
+\gamma_2'(k_x^2+k_y^2-2k_z^2)] & -\frac{C_k}{2}(k_x+ik_y) & -i\sqrt{3}\gamma_3'k_xk_y & & & +i\sqrt{6}\gamma_3'k_xk_y \\
 & & +C_kk_z & & & \\
 & -\frac{1}{2}[\gamma_1k^2 & -\frac{C_k\sqrt{3}}{2}(k_x+ik_y) & \frac{\sqrt{3}}{2}\gamma_2'(k_x^2-k_y^2) & -\frac{\gamma_2'}{\sqrt{2}}(k_x^2+k_y^2-2k_z^2) & \frac{3}{\sqrt{2}}\gamma_3'k_zk_+ \\
 & -\gamma_2(k_x^2+k_y^2-2k_z^2)] & & -i\sqrt{3}\gamma_3'k_xk_y & & \\
 & & & -C_kk_z & & \\
 & & -\frac{1}{2}[\gamma_1'k^2 & -\sqrt{3}\gamma_3'k_zk_+ & \frac{3}{\sqrt{2}}\gamma_3'k_zk_- & \frac{\gamma_2'}{\sqrt{2}}(k_x^2+k_y^2-2k_z^2) \\
 & & -\gamma_2'(k_x^2+k_y^2-2k_z^2)] & -\frac{C_k}{2}(k_x+ik_y) & & \\
 & & & -\frac{1}{2}[\gamma_1'k^2 & \sqrt{3/2}\gamma_2'(k_x^2-k_y^2) & -\sqrt{3/2}\gamma_3'k_zk_- \\
 & & & +\gamma_2'(k_x^2+k_y^2-2k_z^2)] & +i\sqrt{6}\gamma_3'k_xk_y & \\
 & & & & -\frac{1}{2}\gamma_1'k^2-\Delta_0 & 0 \\
 & & & & 0 & -\frac{1}{2}\gamma_1'k^2-\Delta_0
\end{array} \tag{A2}$$

These matrix elements imply a choice of phase in the angular-momentum wave functions which the reader can easily retrace. It is consistent with Ref. 25. As an aid to the reader in constructing the full Hamiltonian matrix, we give below the "diagonal" matrix connecting the Γ_{15}^v states with themselves. That connecting Γ_{15}^c with themselves is isomorphic to it and can be easily written down by inspection. We have used atomic units ($e=\hbar=m=1$). In Eq. (A2) we use $k_+=k_x+ik_y$ and $k_-=k_x-ik_y$.

The Luttinger parameters γ_1, γ_2, and γ_3 are related to P, P', and Q and the residual parameters γ' through the equations[61]

$$\gamma_1 = A + \gamma_1' , \quad \gamma_2 = \frac{B}{2} + \gamma_2' , \quad \gamma_3 = \tfrac{1}{6}(F + H_1) + \gamma_3' , \quad A = \tfrac{1}{3}(F + 2M) + 1 , \quad B = \tfrac{1}{3}(F - M) ,$$
$$C^2 = \tfrac{1}{3}[(F+M)^2 - (F-M)^2] , \quad F = \frac{2P^2}{E_0} , \quad M = \frac{2Q^2}{E_0' + 2\Delta_0'/3} . \tag{A3}$$

[1]See, for instance, J. Chelikovsky and M. L. Cohen, Phys. Rev. B **14**, 5372 (1976).

[2]See, for instance, M. Cardona, K. L. Shaklee, and F. H. Pollak, Phys. Rev. **154**, 696 (1967).

[3]J. C. Phillips, *Bonds and Bands in Semiconductors* (Academic, New York, 1973).

[4]J. Tauc and A. Abraham, in *Proceedings of the International Conference on the Physics of Semiconductors, Prague, 1960* (Czechoslavakian Academy of Science, Prague, 1961), p. 375.

[5]G. Dresselhaus, Phys. Rev. **186**, 824 (1958).

[6]E. O. Kane, in *Semiconductors and Semimetals,* edited by R. K. Willardson and A. C. Beer (Academic, New York, 1966), Vol. 1, pp. 75 and 94.

[7]N. E. Christensen and O. B. Christensen, Phys. Rev. B **33**, 4739 (1986).

[8]M. Cardona, F. H. Pollak, and J. G. Broerman, Phys. Lett. **19**, 276 (1965).

[9]N. E. Christensen and M. Cardona, Solid State Commun. **51**, 491 (1984).

[10]M. Cardona, N. E. Christensen, and G. Fasol, Phys. Rev. Lett. **56**, 2831 (1986).

[11]M. Cardona, N. E. Christensen, and G. Fasol, in *Proceedings of the International Conference on the Physics of Semiconductors, Stockholm 1986,* edited by O. Enström (World Scientific, Singapore, 1987), p. 1133.

[12]M. I. Diakonov and V. I. Perel, in *Optical Orientation,* edited by V. M. Agranovich and A. A. Maradudin (North-Holland, Amsterdam, 1984), p. 11

[13]G. E. Pikus and A. N. Titkov, In Ref. 2, p. 73.

[14]A. T. Gorelenko, B. A. Marushchak, and A. N. Titkov, Izv. Akad. Nauk SSSR, Ser. Fiz. **50**, 290 (1986).

[15]W. Kauschke, N. Mestres, and M. Cardona, Phys. Rev. B **35**, 3843 (1987).

[16]M. A. Alekseev, V. D. Dymnikov, D. N. Mirlin, I. I. Reshina, and V. F. Sapega, Fiz. Tverd. Tela (Leningrad) **28**, 793 (1986) [Sov. Phys.—Solid State **28**, 441 (1986)].

[17]Y. F. Chen, M. Dobrowolska, J. K. Furdyna, and S. Rodriguez, Phys. Rev. B **32**, 890 (1985).

[18]M. Cardona, N. E. Christensen, M. Dobrowolska, J. K. Furdyna, and S. Rodriguez, Solid State Commun. **60**, 171 (1986).

[19]H. Riechert, S. F. Alvarado, A. N. Titkov, and V. I. Safarov, Phys. Rev. Lett. **52**, 2297 (1984).

[20]M. Cardona, V. A. Maruschak, and A. N. Titkov, Solid State Commun. **50**, 701 (1984).

[21]O. K. Andersen, Phys. Rev. B **12**, 3060 (1975).

[22]D. Glötzel, B. Segal, and O. K. Andersen, Solid State Commun. **36**, 403 (1980).

[23]M. S. Hybertsen and S. G. Louie, Phys. Rev. B **34**, 5390 (1986).

[24]F. H. Pollak, C. W. Higginbotham, and M. Cardona, J. Phys. Soc. Jpn. Suppl. **21**, 20 (1966).

[25]U. Rössler, Solid State Commun. **49**, 943 (1984).

[26]M. Cardona, J. Phys. Chem. Solids **24**, 1543 (1963).

[27]R. L. Bowers and G. D. Mahan, Phys. Rev. **185**, 1073 (1969).

[28]P. Lawaetz, Phys. Rev. B **4**, 3460 (1971).

[29]C. Herman and C. Weisbuch, Phys. Rev. B **15**, 8233 (1977); G. W. Pratt and L. G. Ferreira, in *Physics of Semiconductors* (Dunod, Paris, 1964), p. 63.

[30]M. Cardona and F. H. Pollak, Phys. Rev. **142**, 530 (1966).

[31]A. Blacha, H. Presting, and M. Cardona, Phys. Status Solidi B **126**, 11 (1984).

[32]J. M. Luttinger, Phys. Rev. **102**, 1030 (1955).

[33]*Landolt-Börnstein Tables,* edited by O. Madelung, M. Schulz, and H. Weiss (Springer, Berlin, 1982), Vol. 17a.

[34]D. E. Aspnes, C. G. Olson, and D. W. Lynch, Phys. Rev. B **12**, 2527 (1975).

[35]G. Ambrazevicius, M. Cardona, and R. Merlin, Phys. Rev. Lett. **59**, 700 (1987).

[36]M. Cardona, Phys. Rev. B **31**, 7989 (1986).

[37]H. Sigg, J. A. A. J. Perenboom, P. Pfeffer, and W. Zawadzki, Solid State Commun. **61**, 685 (1987).

[38]G. B. Bachelet and N. E. Christensen, Phys. Rev. B **31**, 879 (1985).

[39]L. Brey, N. E. Christensen, and M. Cardona, Phys. Rev. B **36**, 2638 (1987).

[40]K.-H. Weyrich, Phys. Rev. B (to be published).

[41]K.-H. Weyrich, L. Brey, and N. E. Christensen, Phys. Rev. B **38**, 1392 (1988).

[42]N. E. Christensen, J. Phys. F **8**, L51 (1978).

[43]C. Godreche, J. Magn. Magn. Mater. **29**, 263 (1982).

[44]D. M. Ceperley and B. J. Alder, Phys. Rev. Lett. **45**, 566 (1980).

[45]J. Perdew and A. Zunger, Phys. Rev. B **23**, 5048 (1981).

[46]A. H. MacDonald and S. H. Vosko, J. Phys. C **12**, 2977 (1979).

[47]N. E. Christensen, Phys. Rev. B **30**, 5753 (1984).

[48]M. Alouani, L. Brey, and N. E. Christensen, Phys. Rev. B **37**, 1167 (1988).

[49]M. Cardona and N. E. Christensen, Phys. Rev. B **35**, 6182 (1987).

[50]C. W. Higginbotham, Ph.D. thesis, Brown University, 1967 (unpublished).

[51]M. Cardona, *Modulation Spectroscopy* (Academic, New York, 1969).

[52]W. A. Harrison, *Electronic Structure and the Properties of Solids* (Freeman, San Francisco, 1980). In Eq. (4.5) we actually use the parameters of the $3p^3s^*$ model, W. A. Harrison, Phys. Rev. B **24**, 5835 (1981).

[53]See, for instance, G. Koster, *Space Groups and their Representations* (Academic, New York, 1957).

[54]W. Howlett and S. Zukotynski, Phys. Rev. B **16**, 3688 (1977).

[55]X. Z. Lu, M. Dulla, T. Shigenari, and H. Z. Cummins, Phys. Rev. B **32**, 1037 (1985).

[56]D. G. Seiler, B. D. Bajaj, and A. E. Stevens, Phys. Rev. B **16**, 2822 (1977).

[57]R. Ranvaud, F. H. Pollak, U. Rössler, and H. R. Trebin, Phys. Rev. B **20**, 701 (1979).

[58]G. L. Pikus and G. E. Bir, Fiz. Tverd. Tela (Leningrad) **3**, 3050 (1961) [Sov. Phys.—Solid State **3**, 2221 (1962)].

[59]We are grateful to U. Rössler for pointing this out to us.

[60]M. Cardona, J. Res. Nat. Bur. Stand. (U.S.) Ser. A **74**, 253 (1970).

[61]J. Hensel and K. Suzuki, Phys. Rev. B **9**, 4184 (1974).